

Supporting Information

for

**Electrochemical Hydrogenation of a Benzannulated Pyridine to a Dihydropyridine
in Acidic Solution**

Patrick K. Giesbrecht^a, Dion B. Nemez^a and David E. Herbert^{a*}

^a*Department of Chemistry and Manitoba Institute for Materials, University of Manitoba,*

144 Dysart Rd, Winnipeg, Manitoba, Canada R3T 2N2

*david.herbert@umanitoba.ca

TABLE OF CONTENTS

EXPERIMENTAL	2
Chemicals and Reagents	2
Synthesis of 1,2-Dihydrophenanthridine (1-H₂)	2
Electrochemical Methods	2
Isolation of 1-H₂ from a Bulk Electrolyzed Solution	3
Product Analysis	3
NMR Characterization Protocol	3
GC-FID Characterization Protocol	3
UV-Vis Spectroscopy of 1, 1-H₂, and Electrochemically Generated 1-H₂	4
Table S1. Experimentally determined pK_a values for phenanthridine (1) mixed CH₃CN/H₂O solvent systems	4
Table S2. Electrolysis of FA-containing solutions of 1.	5
Transfer Hydrogenation Promoted by Electrochemically Generated 1-H₂	5
REFERENCES	6
CONTROLLED POTENTIAL ELECTROLYSIS PLOTS	6
CYCLIC VOLTAMMETRY	8
GC-FID CHROMATOGRAMS	11
¹H NMR SPECTROSCOPIC ANALYSIS: BEFORE & AFTER BULK ELECTROLYSES	13
UV-VIS SPECTROSCOPY	28

EXPERIMENTAL

Chemicals and Reagents

All chemicals and reagents were used as received unless otherwise noted. Solutions for electrochemical experiments were made using MilliQ water (18.2 $\Omega\cdot\text{cm}$) and HPLC grade CH_3CN (BDH Chemicals), with LiClO_4 (98%, Sigma Aldrich) as the supporting electrolyte. Phenanthridine (**1**, 98%, Acros Organic) was used as received in 1 or 10 mM concentrations in non-aqueous (CH_3CN), and mixed solutions (10%, 60% (v:v) $\text{H}_2\text{O}/\text{CH}_3\text{CN}$). Formic acid (FA, 98% Alfa Aesar), acetic acid (AA), and perchloric acid (HClO_4) were used as received in 3 to 1000 mM concentrations. LiAlH_4 (Sigma) and diethyl ether (Sigma Aldrich) were used as received for synthesis of **1-H₂**. Tetrahydrofuran (THF) was dried using sodium wire (with benzophenone indicator) prior to use.

Synthesis of 1,2-Dihydrophenanthridine (**1-H₂**)

The synthesis of 1,2-dihydrophenanthridine (**1-H₂**) was adapted from a previous report.^[1] In brief, a nitrogen-purged solution of LiAlH_4 (0.508 g, 13.4 mmol) in THF (7 mL) was added drop-wise to a solution of **1** (0.400 g, 2.22 mmol) in THF (10 mL) under nitrogen, and the resulting green mixture stirred at room temperature for 16 h. The solution was then cooled to 0 °C and 7 mL of argon-purged water was added. The mixture was kept at this temperature for 1 h then warmed to room temperature, at which point any solid was filtered off and the filtrate dried to give a yellow white powder. Yield = 0.350 g (87%, >95% pure). ^1H NMR (300 MHz, CDCl_3 , 22 °C): δ 7.72 ppm (dd and d overlapping, $J = 7.80$ Hz, $J = 7.50$, 1.50 Hz 2H, aromatic *CH*); 7.34 (td, $J = 1.48$, 7.58, 7.75 Hz, 1H, aromatic *CH*); 7.25 (td, $J = 1.33$, 7.41, 7.38 Hz, 1H, aromatic *CH*); 7.14 (m, 2H, aromatic *CH*); 6.87 (td, $J = 1.22$, 7.56, 7.58 Hz, 1H, aromatic *CH*); 6.69 (dd, $J = 1.20$, 7.96 Hz, 1H, aromatic *CH*); 4.42 (singlet, 2H, *CH*₂); 3.99 ppm (broad singlet, 1H, *NH*). ^{13}C { ^1H } NMR (75 MHz, CDCl_3 , 22 °C): δ 145.83 (*C*_{Ar}), 132.86 (*C*_{Ar}), 132.20 (*C*_{Ar}), 128.92 (*C*_{Ar}), 127.77 (*C*_{Ar}), 127.24 (*C*_{Ar}), 126.12 (*C*_{Ar}), 123.70 (*C*_{Ar}), 122.53 (*C*_{Ar}), 122.17 (*C*_{Ar}), 119.38 (*C*_{Ar}), 115.23 (*C*_{Ar}), 46.50 (*CH*₂) ppm.

Electrochemical Methods

CV experiments were performed on a CHI 760c bipotentiostat at scan rates of 50 to 800 mV s^{-1} using freshly polished (0.05 μm alumina paste) Pt or glassy carbon (GCE) disc working electrodes, a Pt wire counter electrode, and a Ag/AgCl aqueous quasi-reference electrode. Ferrocene (FcH) was added as an internal standard to each solution upon completion of each set of cyclic voltammetry experiments, allowing potentials to be referenced to the ferrocene/ferrocenium ($\text{FcH}^{0/+}$) redox couple. To account for the use of a mixed solvent system, any shift of the $\text{FcH}^{0/+}$ redox couple due to the $\text{CH}_3\text{CN}/\text{H}_2\text{O}$ ratio employed was considered, as previously described.^[2]

Potentiostatic bulk electrolyses were conducted using a Pt mesh electrode (125 cm^2) and a reticulated vitreous carbon (RVC) electrode (~ 700 cm^2) with Ar constantly bubbled into the solution (1 atm) and the solution stirred, with a graphite rod counter

electrode in a fritted tube and a Ag/AgCl quasi-reference electrode (total volume of 90 mL). Potentials in the range of -0.50 to -1.1 V vs. Ag/AgCl were applied, for approximately 10 000 s.

Isolation of 1-H₂ from a Bulk Electrolyzed Solution

Using one of the optimized conditions for DHP formation (see Table 1 of the manuscript), 45 mg of **1** was placed into a 60 % (v:v) H₂O/CH₃CN in the presence of 10 mM FA (total volume of 90 mL, 2 mM **1**) and electrolyzed extensively with $E_{\text{applied}} = -0.83$ V vs. FcH^{0/+} at a Pt electrode. After electrolysis, the electrode was washed with 20 mL CH₃CN, and the solvent removed under reduced pressure at 40 °C. A dichloromethane extraction (20 mL) was conducted, with water washings (3 x 10 mL), dried using sodium sulfate and filtered over celite. The dichloromethane was removed under reduced pressure to provide a yellow-orange solid (41 mg, 91% yield, 89% conversion). Comparison of ¹H NMR, ¹³C{¹H} NMR and HSQC-DEPT with those of **1** and **1-H₂** afforded identification of the product to be **1-H₂** (Figures S34-43).

Product Analysis

Reduction of FA by platinum and glassy carbon electrodes in the absence of added ANH was also investigated, with no methanol generation observed under the experimental conditions employed (Figure S15). All bulk electrolyses at Pt and RVC electrodes were conducted a minimum of two times, with no increase or decrease in methanol content observed over a storage period of one month. Thus, we conclude that any methanol is a result of bulk electrolysis of FA in the presence of ANHs rather than a contaminant in the systems used in this work.

NMR Characterization Protocol

¹H NMR spectroscopic analyses were performed on a 500 MHz spectrometer (Bruker) using aliquots (0.6 mL) taken directly from the electrolyzed solution and mixed with 0.06 mL CD₃CN. A pulse sequence suppression was applied to peaks attributed to H₂O (~3.1 ppm) and CH₃CN (~2.0 ppm) peaks, with a delay time of 3.0 s, a 12 μs pulse width, and 0.82 s acquisition time. Due to the large water peak appearing in the methanol peak region, methanol quantification could not be conducted using ¹H NMR spectroscopy.

GC-FID Characterization Protocol

Methanol quantification was conducted using GC-FID. Prior to injection into the GC, the electrolyzed solution was desalted by a bulb-to-bulb transfer of the volatiles. A 1.0 μL aliquot of the desalted solution in a 1/10 split was then injected into the GC, with the headspace heated to 250 °C and a Supelco Wax column heated at 50 °C for 3 min, raised to 160 °C over 9 min, and maintained for another 4 min, at a flow rate of 1 mL/min. Methanol content was determined by analyzing the peak produced at a retention time of 6.7 to 6.9 min in the chromatogram, as determined from standard solutions, using CompassCDS 3.0 Software (Bruker) (solvent peak arises at 8.5 min). A linear baseline correction was used for all GC-FID peak integrations conducted in this work, with the peak area determined for each sample to be in the range of 0.8-6.0 μV*min, and with an error of 0.6 μV*min (corresponding to integrating the noise in the blank samples at 6.8

min, 10-80% of the corresponding peak area in the bulk electrolysis samples) from the integration method used.

To ensure the signal attributed to methanol was not the result of contamination from the bulb-to-bulb transfer or the bulk electrolysis procedure, bulk electrolysis of control solutions with no ANH/DHP added were subjected to the bulb-to-bulb transfer protocol and run using the same GC-FID method, with no discernable signal registered (Figure S15).

To address concerns over the sensitive nature of this analytical technique to pre-treatment of the instruments and the low concentrations generated from bulk electrolysis, a CH₃CN blank was passed through the column in quintuplicate before and after analyses of electrolysis (run first) and standard solutions, respectively.

Concentration of MeOH was determined through comparison to an external calibration curve (Figure S12). To account for any drift associated with the instrument, the retention times for MeOH were determined through comparison to a standard each day samples were run.

UV-Vis Spectroscopy of **1**, **1-H₂**, and Electrochemically Generated **1-H₂**

UV-Vis Spectroscopy of **1**, **1-H₂** chemically synthesized, and **1-H₂** electrochemically generated was conducted in the range of 190-1100 nm (Bruker), with the ANH/DHP solutions in 10⁻⁵-10⁻⁶ M concentrations in CH₃CN. To ensure accurate determination of the identity of the species electrochemically generated, the spectra were normalized to the peak occurring at 243 nm (Figure S44).

Table S1. Experimentally determined p*K*_a values for phenanthridine (**1**) mixed CH₃CN/H₂O solvent systems.

ANH	p <i>K</i> _a in 60% (v:v) H ₂ O/CH ₃ CN ¹	p <i>K</i> _a in 10% (v:v) H ₂ O/CH ₃ CN
Phenanthridine (1)	3.6	2.6

¹Ref. 3.

Table S2. Electrolysis of FA-containing solutions of **1**.

Entry	1:FA ^a	E _{applied} ^b	Solvent ^c	1-H ₂ (%) ^d	%FE ^e 1-H ₂	[MeOH] ^f	%FE ^g MeOH	pH ^h
1	1:10	-1.23 (Pt)	10%	43(5)	3.2(0.6)	35(1)	0.55(0.11)	3.76
2	1:100	-1.23 (Pt)	10%	49(11)	2.6(0.6)	30(3)	0.34(0.03)	3.23
3	1:1000	-1.23 (Pt)	10%	80(1)	3.5(0.6)	73(7)	0.63(0.04)	2.05
4	1:10	-1.23 (Pt)	60%	99(1)	5.4(0.1)	28(1)	0.31(0.01)	3.22
5	1:10	-0.83 (Pt)	10%	5(2)	5.2(1.5)	ND	-	3.76
6	1:10	-0.83 (Pt)	60%	36(10)	19(6)	23(5)	2.1(1.1)	3.22
7	1:10	-1.23 (RVC)	10%	35(10)	21(8)	27(2)	3.2(0.1)	3.76
8	1:10	-1.43 (RVC)	10%	86(8)	40(1)	28(12)	2.8(1.4)	3.76
9	1:10	-1.23 (RVC)	60%	95(2)	71(10)	31(2)	3.6(1.5)	3.22
10	1:100	-1.23 (RVC)	10%	90(2)	18.2(3)	29(11)	1.1(0.2)	3.23
11	1:1000	-1.23 (RVC)	10%	87(7)	6.0(0.7)	76(25)	1.2(0.6)	2.05

^a in mM ^b in V vs. FcH^{0/+}; RVC = reticulated vitreous carbon (glassy carbon). ^c % (v:v) H₂O/CH₃CN. ^d % conversion as determined by ¹H NMR analysis of aliquots from post-electrolysis reaction mixtures. Shown with standard deviation. ^e Faradaic Efficiency of DHP formation. Shown with standard deviation. ^f in μM as determined by GC-FID analysis. Shown with standard deviation. ^g Faradaic Efficiency of Methanol formation. Shown with standard deviation. ^h pH of solution pre-electrolysis.

Transfer Hydrogenation Promoted by Electrochemically Generated 1-H₂

A solution of **1** (0.062 g, 0.35 mmol) was subjected to controlled-potential electrolysis as per run 7, Table 1 (60% v:v H₂O:CH₃CN, 10 equivalents FA, E_{applied} = -1.1 V vs Ag/AgCl, 2 h). An aliquot taken from the electrolysis mixture showed high conversion (99%) to **1-H₂**. The electrolysis mixture was transferred under a positive pressure of argon to a flask containing 3-phenyl-2H-1,4-benzoxazine (0.030 g, 0.14 mmol) and the mixture was stirred at room temperature. After 36 h, all volatiles were removed and the residue extracted with CH₂Cl₂ (2 x 15 mL), filtered and dried *in vacuo*. ¹H NMR analysis of the crude material confirmed full conversion to the known compound 3-phenyl-3,4-dihydro-2H-1,4-benzoxazine (Figure S45) and the product was isolated (0.011 g, 0.05 mmol) as a pale yellow oil using column chromatography R_f = 0.80 (petroleum ether/EtOAc 9/1). Yield = 36%. Spectroscopic data (Figure S46) was matched to the literature.^[4] ¹H NMR (300 MHz, CDCl₃): δ 7.42-7.34 (overlapped m, 5H), 6.85 (dd, J_{HH} = 7.85, 1.39 Hz; 1H, Ar CH), 6.81 (dt, J_{HH} = 7.60, 1.27 Hz; 1H, Ar CH), 6.72-6.67 (overlapped m, 2H, Ar CH), 4.52 (dd, J_{HH} = 8.04, 2.57 Hz, 1H), 4.29 (ddd, J_{HH} = 10.6, 3.0, 1.7 Hz; 1H), 4.01 ppm (dd, J_{HH} = 10.6, 8.6 Hz; 2H).

REFERENCES

- [1] Tanner, D. D.; Yang, C. M. *J. Org. Chem.* 1993, **58**, 1840.
[2] Lanning, J. A.; Chambers, J. Q. *Anal. Chem.* 1973, **45**, 1010.
[3] Giesbrecht, P. K.; Herbert, D. E. *ACS Energy Lett.* 2017, **2**, 549.
[4] Chen, Q.-A.; Gao, K.; Duan, Y.; Ye, Z.-S.; Shi, L.; Yang, Y.; Zhou, Y.-G. *J. Am. Chem. Soc.* 2012, **134**, 2442.

CONTROLLED POTENTIAL ELECTROLYSIS PLOTS

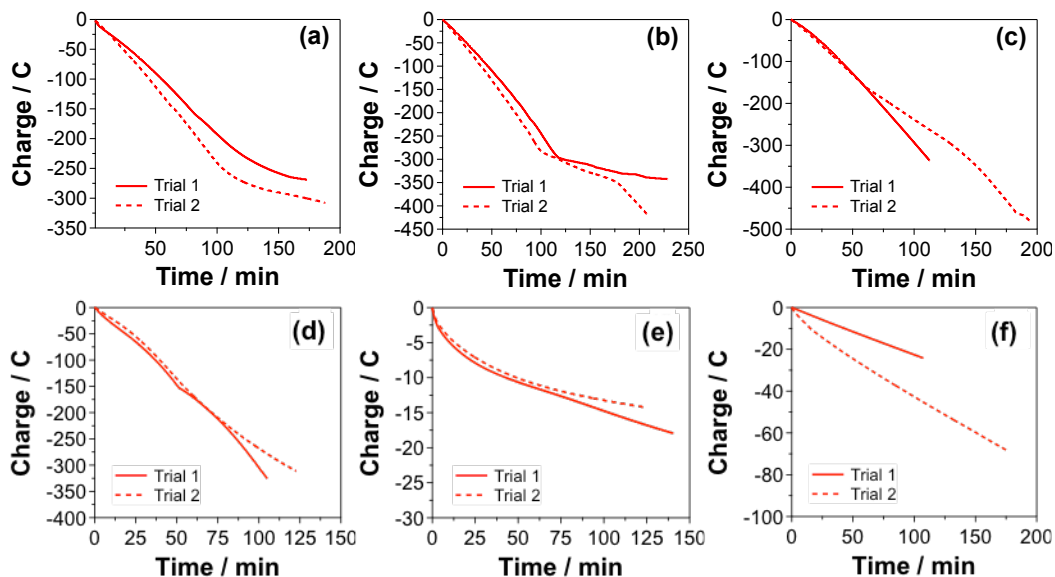


Figure S1. CPE plots for (a) 1 mM **1**: 10 mM FA (b) 1 mM **1**: 100 mM FA (c) 1 mM **1**: 1000 mM FA in 10% (v:v) H₂O/CH₃CN (d) 1 mM **1**: 10 mM FA in 60% (v:v) H₂O/CH₃CN with $E_{\text{applied}} = -1.23$ V vs. FcH^{0/+}; (e) 1 mM **1**: 10 mM FA in 10% (v:v) H₂O/CH₃CN (f) 1 mM **1**: 10 mM FA in 60% (v:v) H₂O/CH₃CN, $E_{\text{applied}} = -0.83$ V vs. FcH^{0/+}. 0.1 M LiClO₄; Pt mesh electrode.

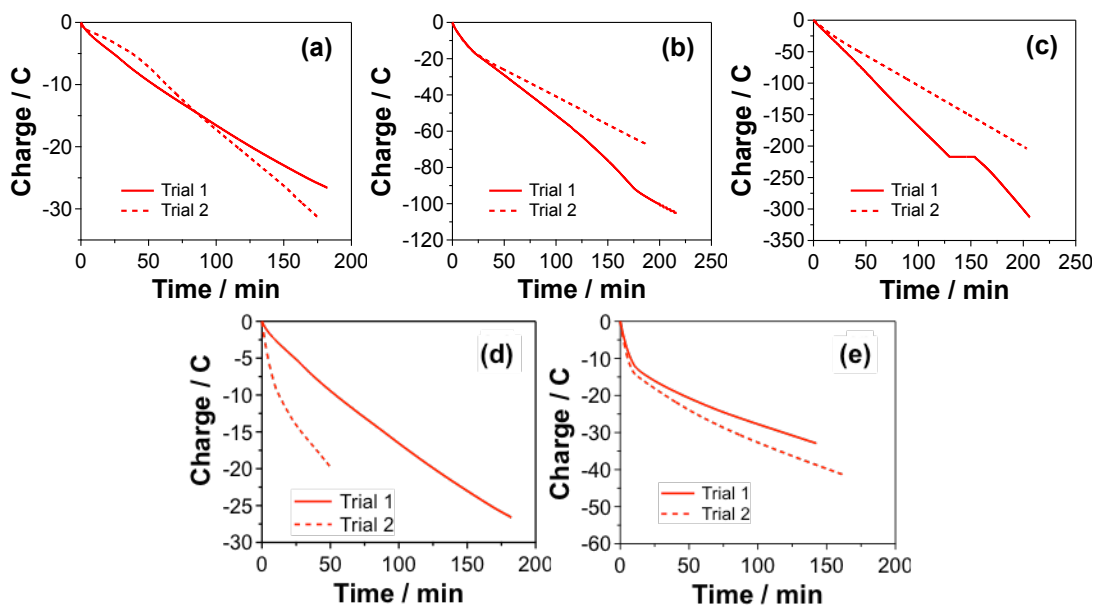


Figure S2. CPE plots for (a) 1 mM **1**: 10 mM FA (b) 1 mM **1**: 100 mM FA (c) 1 mM **1**: 1000 mM FA in 10% (v:v) H₂O/CH₃CN; (d) 1 mM **1**: 10 mM FA in 60% (v:v) H₂O/CH₃CN with $E_{\text{applied}} = -1.23$ V vs. FcH^{0/+}; and (e) 1 mM **1**: 10 mM FA in 10% (v:v) H₂O/CH₃CN with $E_{\text{applied}} = -1.43$ V vs. FcH^{0/+}. 0.1 M LiClO₄; RVC mesh electrode.

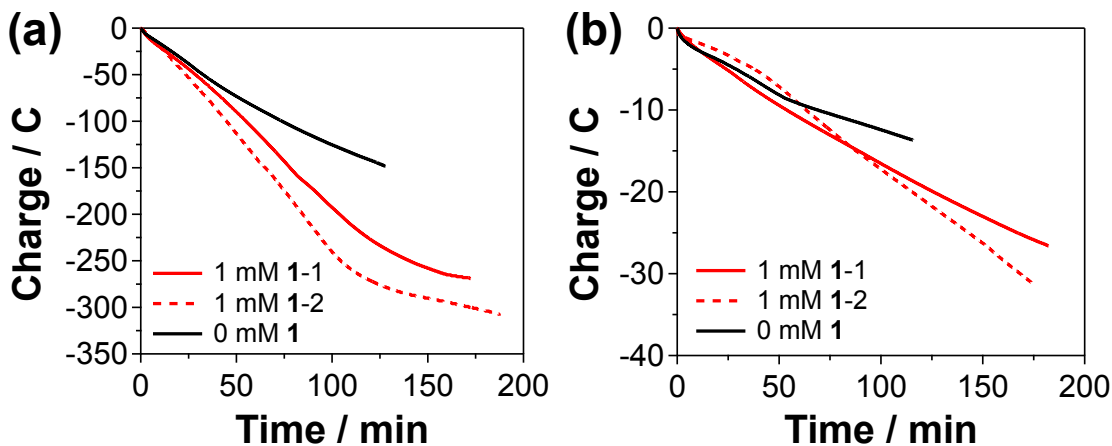


Figure S3. CPE plots for 10 mM FA at (a) Pt and (b) RVC mesh electrodes in the absence (black) and presence of 1 mM **1** for multiple trials (red traces). $E_{\text{applied}} = -1.23$ V vs. FcH^{0/+}; 0.1 M LiClO₄; 10% (v:v) H₂O/CH₃CN.

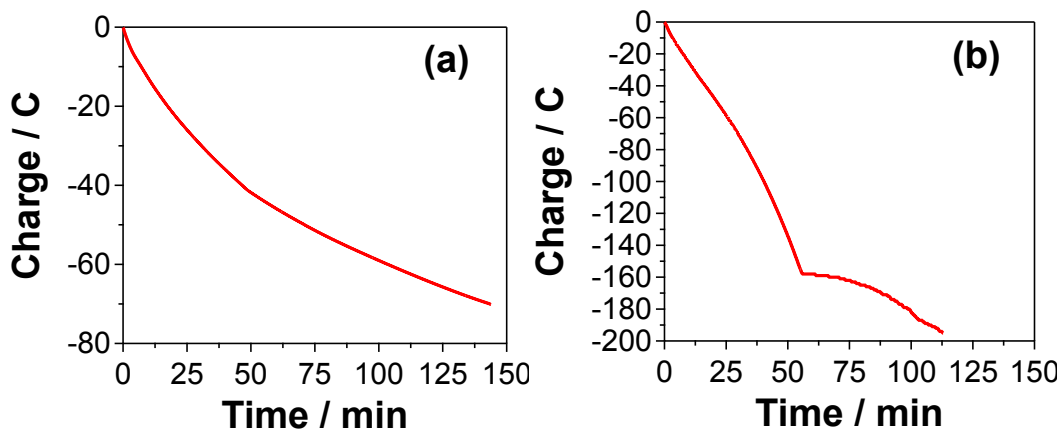


Figure S4. CPE plots for (a) 10 mM **1**: 30 mM AA and (b) 10 mM **1**: 30 mM HClO₄ in 60% (v:v) H₂O/CH₃CN at a Pt mesh electrode. 0.1 M LiClO₄; $E_{\text{applied}} = -0.83$ V vs. FcH^{0/+}.

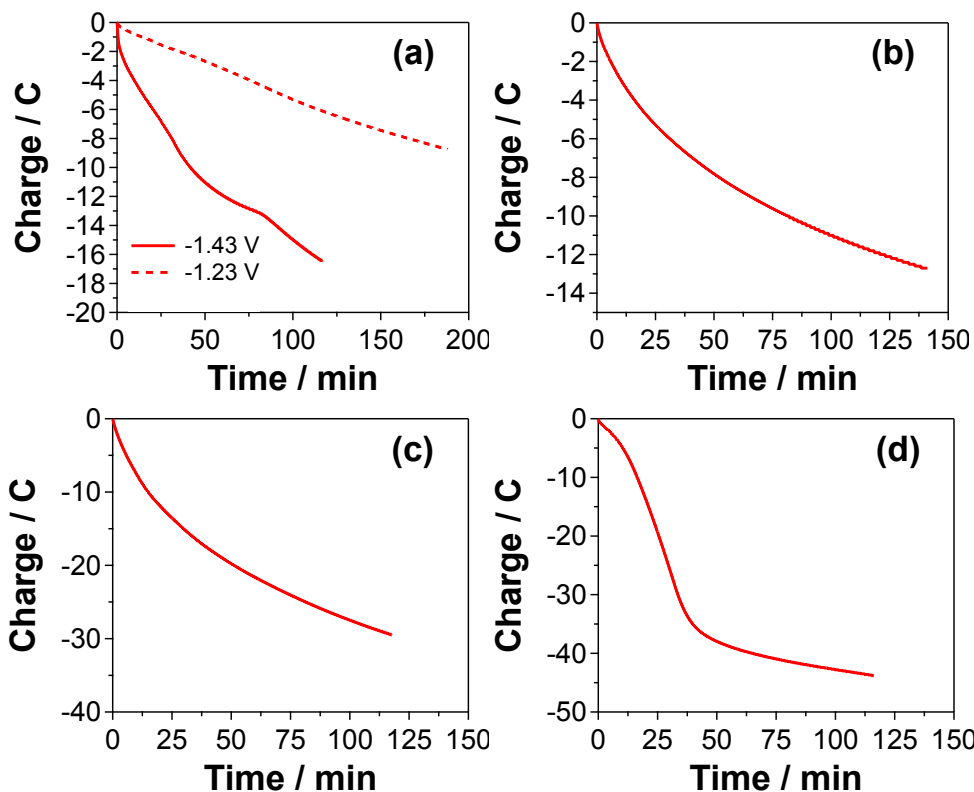


Figure S5. CPE plots for (a) 1 mM **1**: 3 mM AA at $E_{\text{applied}} = -1.23$ V vs. $\text{FcH}^{0/+}$ and $E_{\text{applied}} = -1.43$ V vs. $\text{FcH}^{0/+}$ in CH_3CN , (b) 1 mM **1**: 3 mM AA at $E_{\text{applied}} = -1.23$ V vs. $\text{FcH}^{0/+}$ in 60% (v:v) $\text{H}_2\text{O}/\text{CH}_3\text{CN}$, (c) 1 mM **1**: 3 mM AA at $E_{\text{applied}} = -1.43$ V vs. $\text{FcH}^{0/+}$ in 10% (v:v) $\text{H}_2\text{O}/\text{CH}_3\text{CN}$, (d) 1 mM **1**: 3 mM HClO_4 at $E_{\text{applied}} = -1.23$ V vs. $\text{FcH}^{0/+}$ in 60% (v:v) $\text{H}_2\text{O}/\text{CH}_3\text{CN}$ at a RVC mesh electrode. 0.1 M LiClO_4 .

CYCLIC VOLTAMMETRY

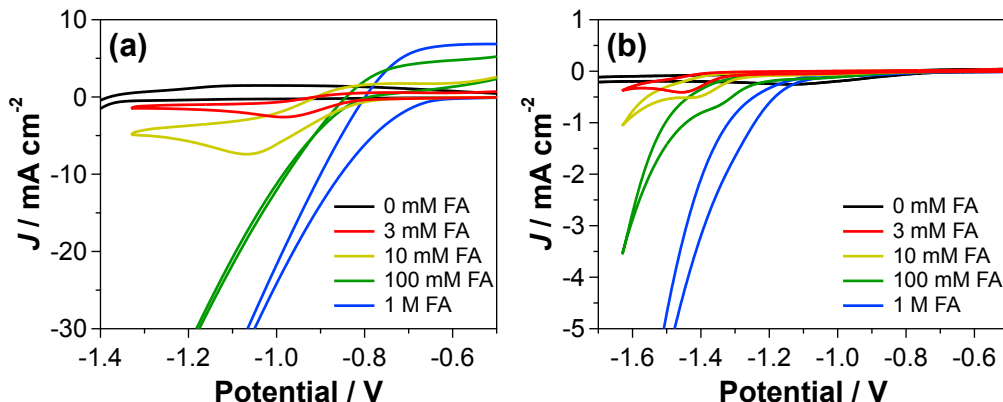


Figure S6. CVs of 1 mM **1** in the presence of 3, 10, 100, 1000 equivalents of FA (FA) at (a) Pt and (b) RVC disc electrodes at 100 mV s^{-1} . 10% (v:v) $\text{H}_2\text{O}/\text{CH}_3\text{CN}$; 0.1 M LiClO_4 ; Potential vs. $\text{FcH}^{0/+}$.

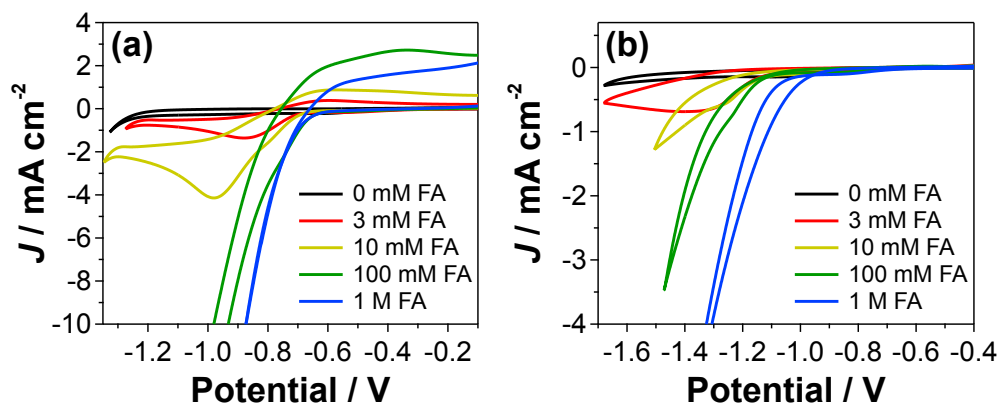


Figure S7. CVs of 1 mM **1** in the presence of 3, 10, 100, 1000 equivalents of FA (FA) at (a) Pt and (b) RVC disc electrodes at 100 mV s^{-1} . 60% (v:v) $\text{H}_2\text{O}/\text{CH}_3\text{CN}$; 0.1 M LiClO_4 ; Potential vs. $\text{FcH}^{0/+}$.

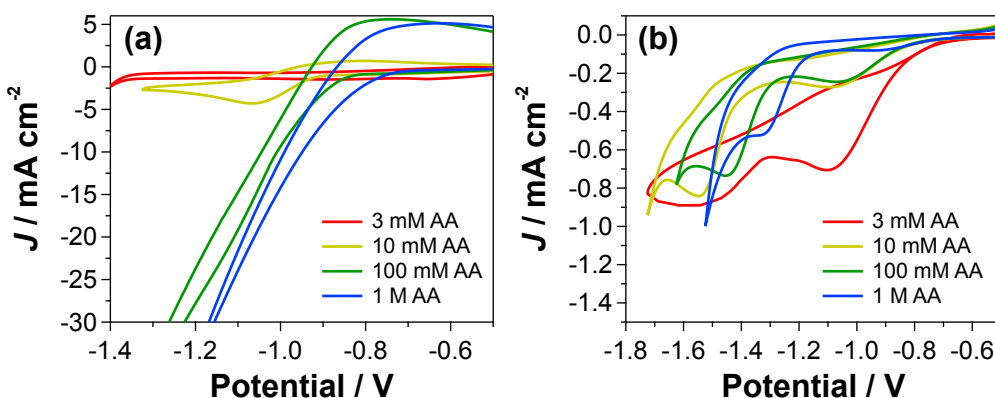


Figure S8. CVs of 1 mM **1** in the presence of 3, 10, 100, 1000 equivalents of AA at (a) Pt and (b) RVC disc electrodes at 100 mV s^{-1} . 10% (v:v) $\text{H}_2\text{O}/\text{CH}_3\text{CN}$; 0.1 M LiClO_4 ; Potential vs. $\text{FcH}^{0/+}$.

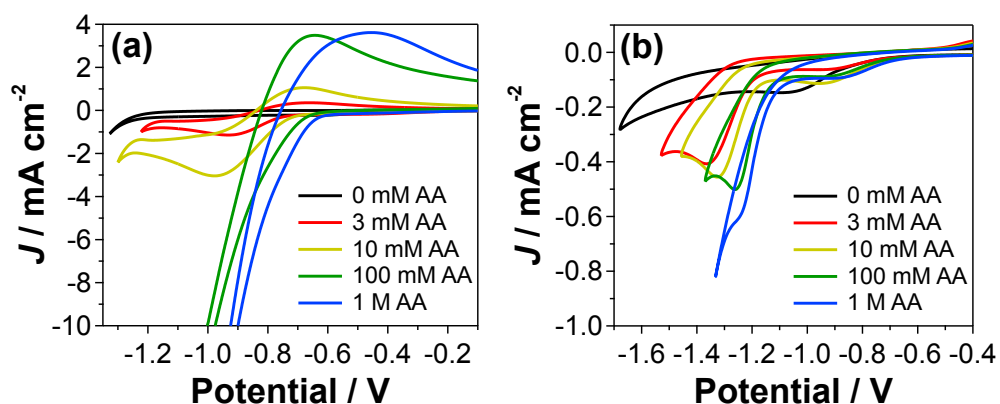


Figure S9. CVs of 1 mM **1** in the presence of 3, 10, 100, 1000 equivalents of AA at (a) Pt and (b) RVC disc electrodes at 100 mV s^{-1} . 60% (v:v) $\text{H}_2\text{O}/\text{CH}_3\text{CN}$; 0.1 M LiClO_4 ; Potential vs. $\text{FcH}^{0/+}$.

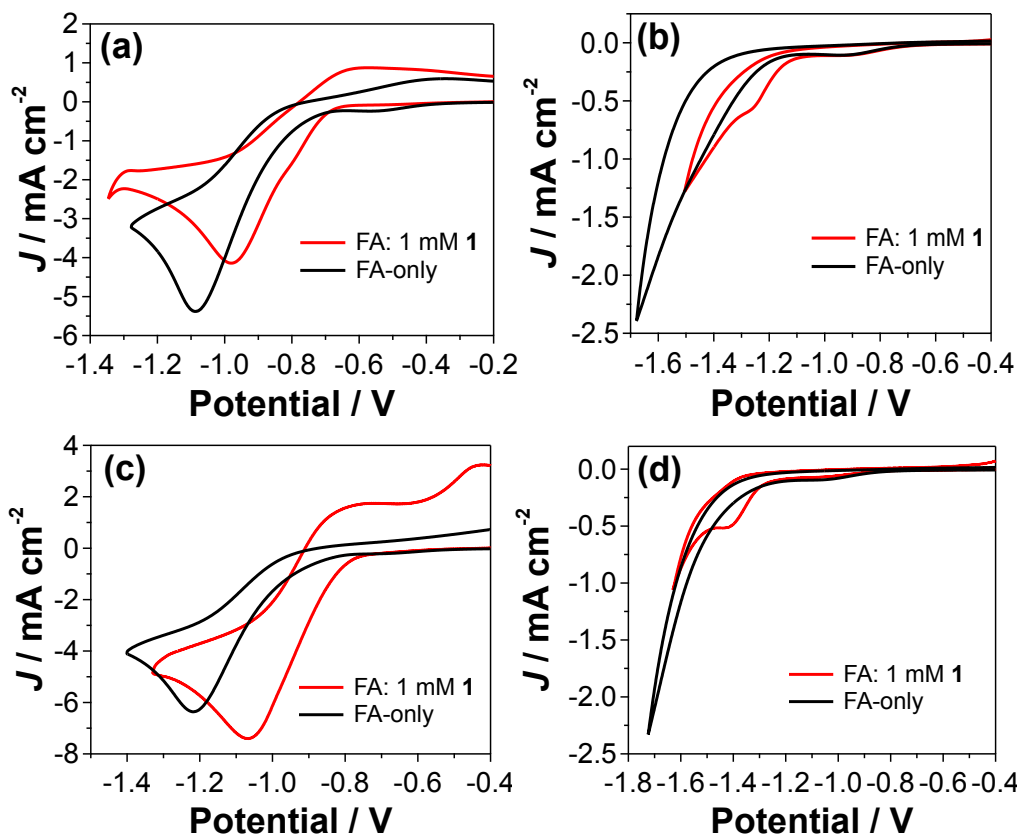


Figure S10. CV comparison of 10 mM FA with and without 1 mM **1** added at (a) Pt and (b) RVC disc electrodes in 60% (v:v) $\text{H}_2\text{O}/\text{CH}_3\text{CN}$; and (c) Pt and (d) RVC disc electrodes in 10% (v:v) $\text{H}_2\text{O}/\text{CH}_3\text{CN}$. Scan rate 100 mV s^{-1} ; 0.1 M LiClO_4 ; Potential vs. $\text{FcH}^{0/+}$.

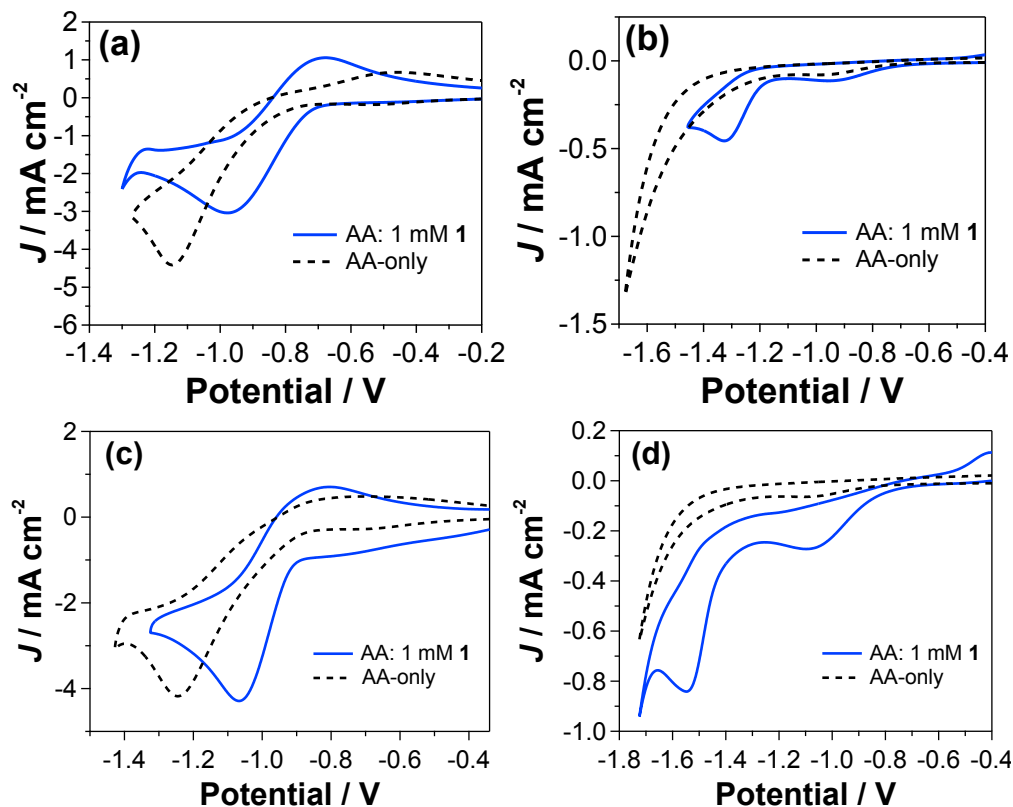


Figure S11. CV comparison of 10 mM AA with and without 1 mM **1** added at (a) Pt and (b) RVC disc electrodes in 60% (v:v) $\text{H}_2\text{O}/\text{CH}_3\text{CN}$; and (c) Pt and (d) RVC disc electrodes in 10% (v:v) $\text{H}_2\text{O}/\text{CH}_3\text{CN}$. Scan rate 100 mV s^{-1} ; 0.1 M LiClO_4 ; Potential vs. $\text{FcH}^{0/+}$.

GC-FID CHROMATOGRAMS

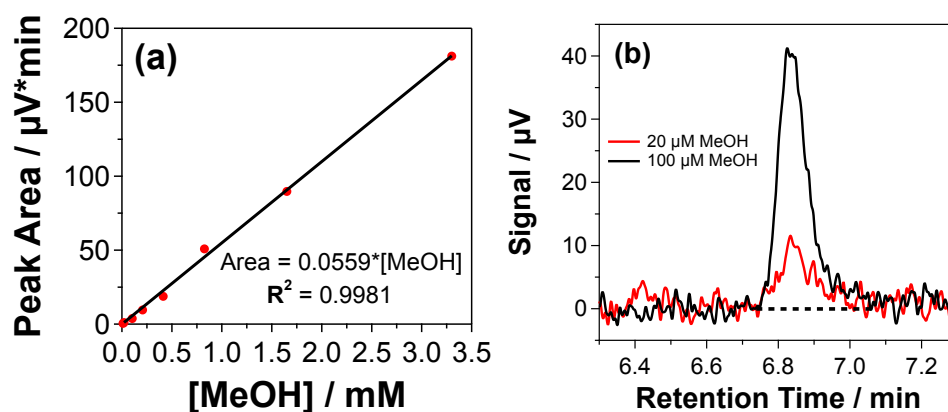


Figure S12. (a) Calibration curve of GC-FID Peak Area versus Concentration of MeOH. (b) Corresponding GC-FID chromatograms for 20 and $100 \mu\text{M MeOH}$ in 10% (v:v) $\text{H}_2\text{O}/\text{CH}_3\text{CN}$. Dashed line indicates baseline used for peak integration.

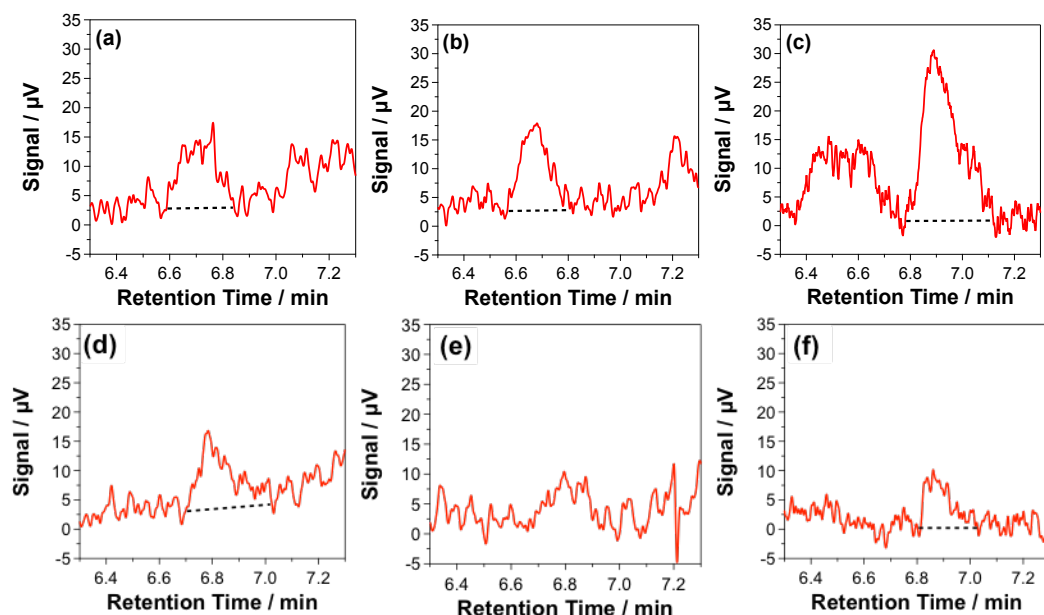


Figure S13. GC-FID chromatograms of bulk electrolysis samples at Pt mesh electrodes for (a) 1 mM **1**: 10 mM FA (b) 1 mM **1**: 100 mM FA (c) 1 mM **1**: 1000 mM FA in 10% (v:v) H₂O/CH₃CN (d) 1 mM **1**: 10 mM FA in 60% (v:v) H₂O/CH₃CN with $E_{\text{applied}} = -1.23$ V vs. FcH^{0/+}; (e) 1 mM **1**: 10 mM FA in 10% (v:v) H₂O/CH₃CN (f) 1 mM **1**: 10 mM FA in 60% (v:v) H₂O/CH₃CN, $E_{\text{applied}} = -0.83$ V vs. FcH^{0/+}. Dashed line indicates baseline used for peak integration.

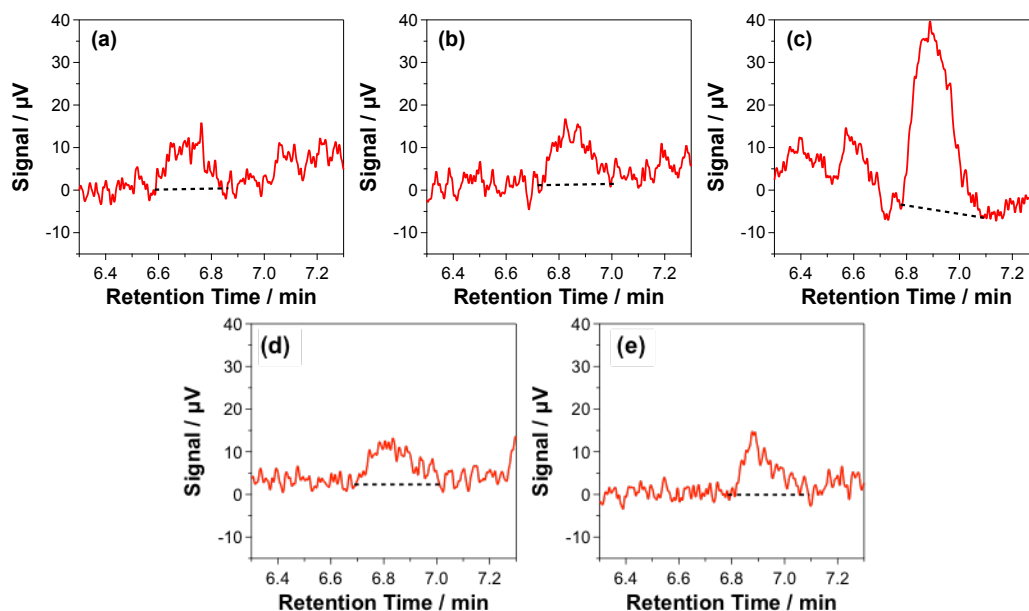


Figure S14. GC-FID Chromatograms of bulk electrolysis samples run at RVC mesh electrodes for (a) 1 mM **1**: 10 mM FA (b) 1 mM **1**: 100 mM FA (c) 1 mM **1**: 1000 mM FA in 10% (v:v) H₂O/CH₃CN; (d) 1 mM **1**: 10 mM FA in 10% (v:v) H₂O/CH₃CN with $E_{\text{applied}} = -1.43$ V vs. FcH^{0/+}; and (e) 1 mM **1**: 10 mM FA in 60% (v:v) H₂O/CH₃CN with $E_{\text{applied}} = -1.23$ V vs. FcH^{0/+}. Dashed line indicates baseline used for peak integration.

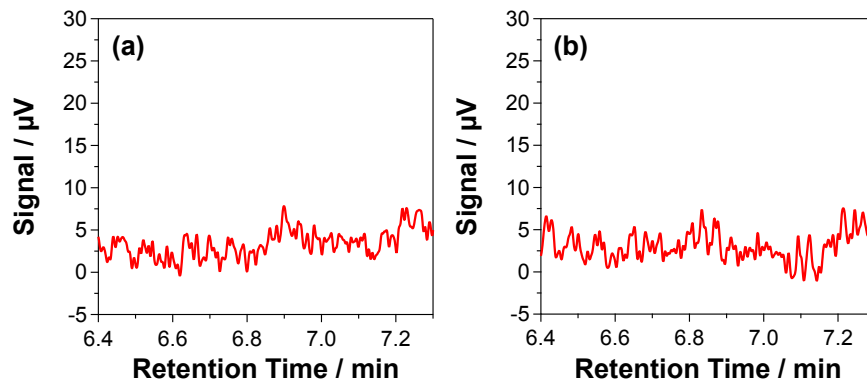


Figure S15. GC-FID Chromatograms of bulk electrolysis control samples run at (a) Pt and (b) RVC mesh electrodes for 10 mM FA, $E_{\text{applied}} = -1.23 \text{ V vs. FcH}^{0/+}$; 10% (v:v) $\text{H}_2\text{O}/\text{CH}_3\text{CN}$. No MeOH observed.

^1H NMR SPECTROSCOPIC ANALYSIS: BEFORE & AFTER BULK ELECTROLYSES

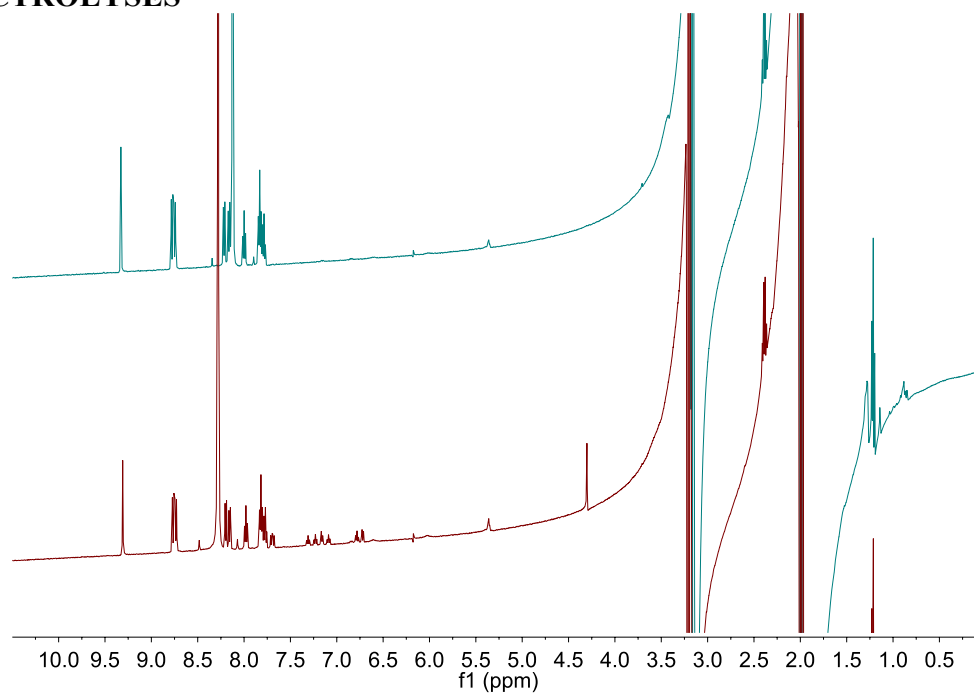


Figure S16. ^1H NMR before (blue, top) and after (red, bottom) bulk electrolysis for 1 mM **1**: 10 mM FA at Pt mesh electrode; $E_{\text{applied}} = -1.23 \text{ V vs. FcH}^{0/+}$; 10% (v:v) $\text{H}_2\text{O}/\text{CH}_3\text{CN}$.

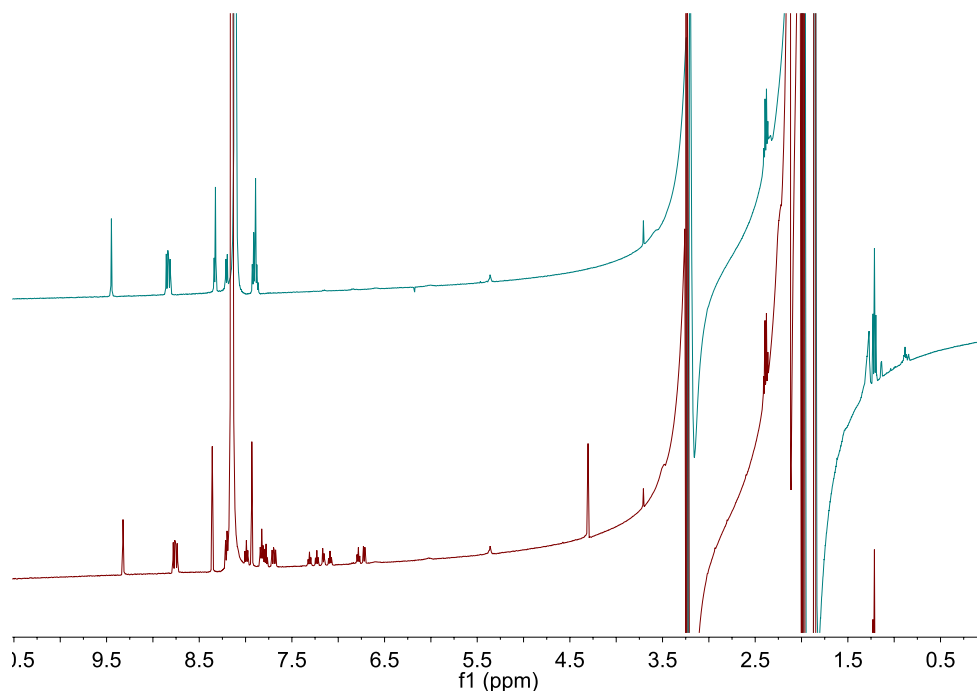


Figure S17. ^1H NMR before (blue, top) and after (red, bottom) bulk electrolysis for 1 mM **1** and 100 mM FA at Pt mesh electrode; $E_{\text{applied}} = -1.23$ V vs. $\text{FcH}^{0/+}$; 10% (v:v) $\text{H}_2\text{O}/\text{CH}_3\text{CN}$.

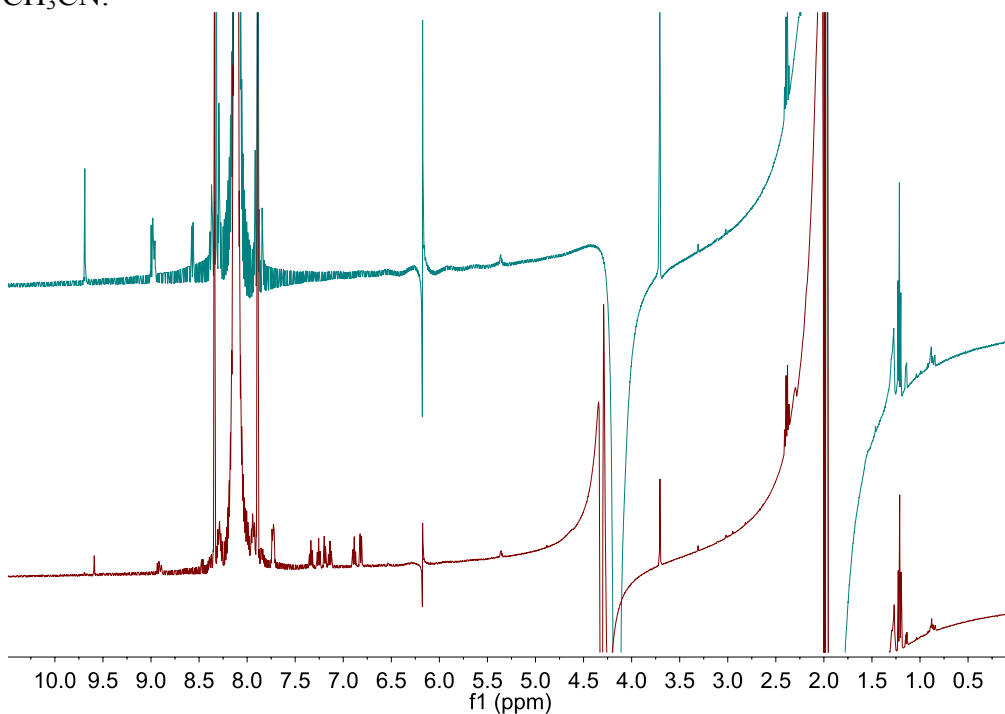


Figure S18. ^1H NMR before (blue, top) and after (red, bottom) bulk electrolysis for 1 mM **1**: 1000 mM FA at Pt mesh electrode; $E_{\text{applied}} = -1.23$ V vs. $\text{FcH}^{0/+}$; 10% (v:v) $\text{H}_2\text{O}/\text{CH}_3\text{CN}$.

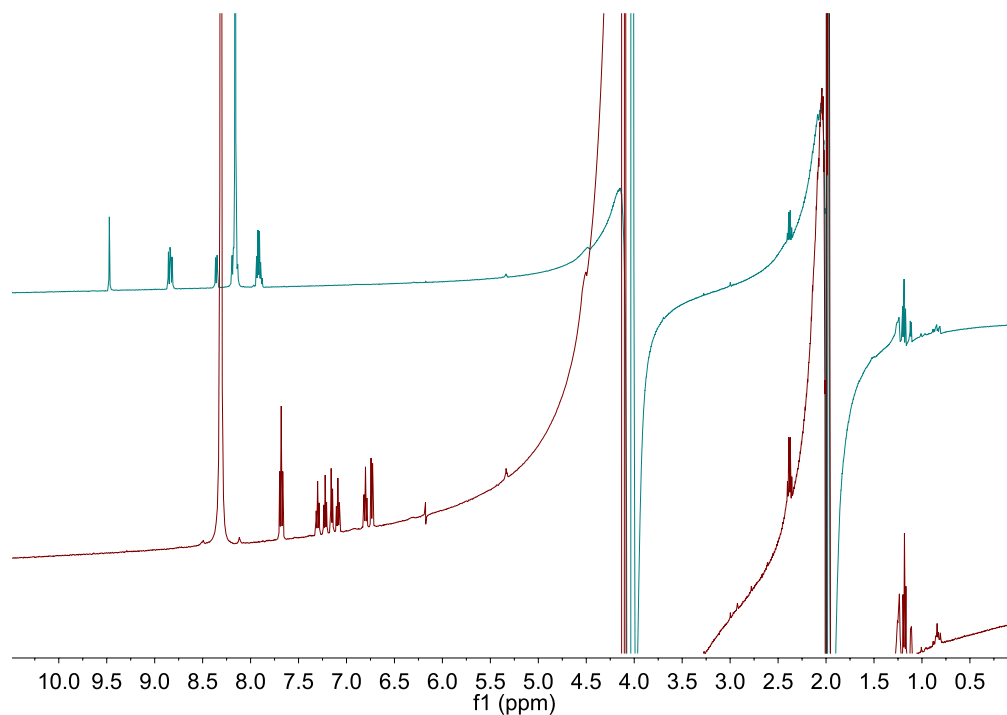


Figure S19. ^1H NMR before (blue, top) and after (red, bottom) bulk electrolysis for 1 mM **1**: 10 mM FA at Pt mesh electrode; $E_{\text{applied}} = -1.23$ V vs. $\text{FcH}^{0/+}$; 60% (v:v) $\text{H}_2\text{O}/\text{CH}_3\text{CN}$.

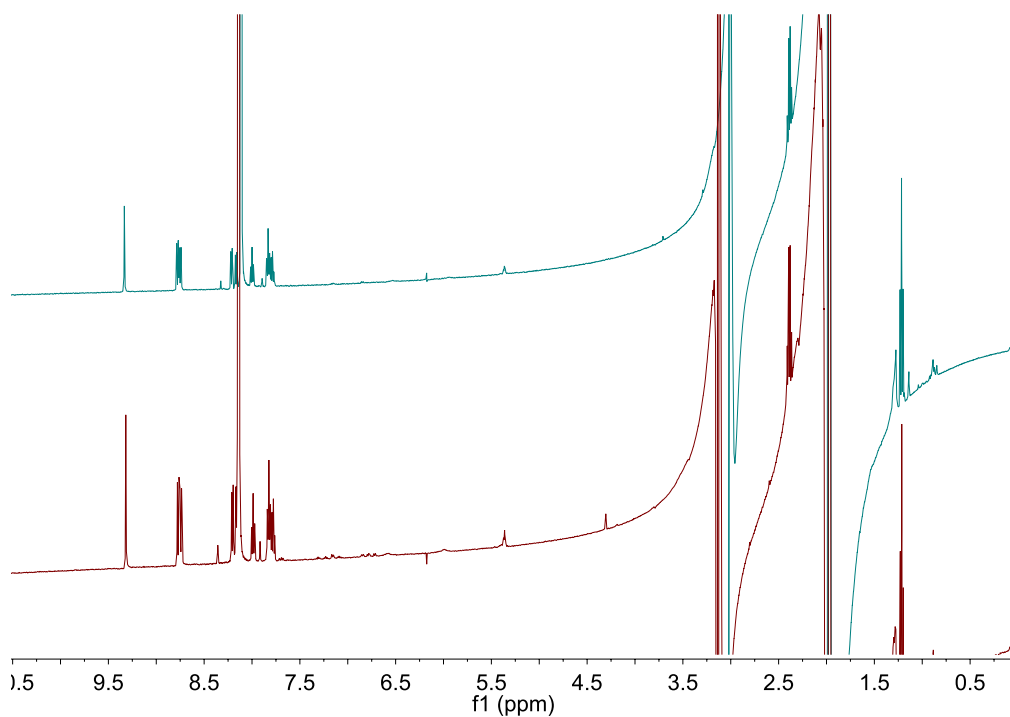


Figure S20. ^1H NMR before (blue, top) and after (red, bottom) bulk electrolysis for 1 mM **1**: 10 mM FA at Pt mesh electrode; $E_{\text{applied}} = -0.83$ V vs. $\text{FcH}^{0/+}$; 10% (v:v) $\text{H}_2\text{O}/\text{CH}_3\text{CN}$.

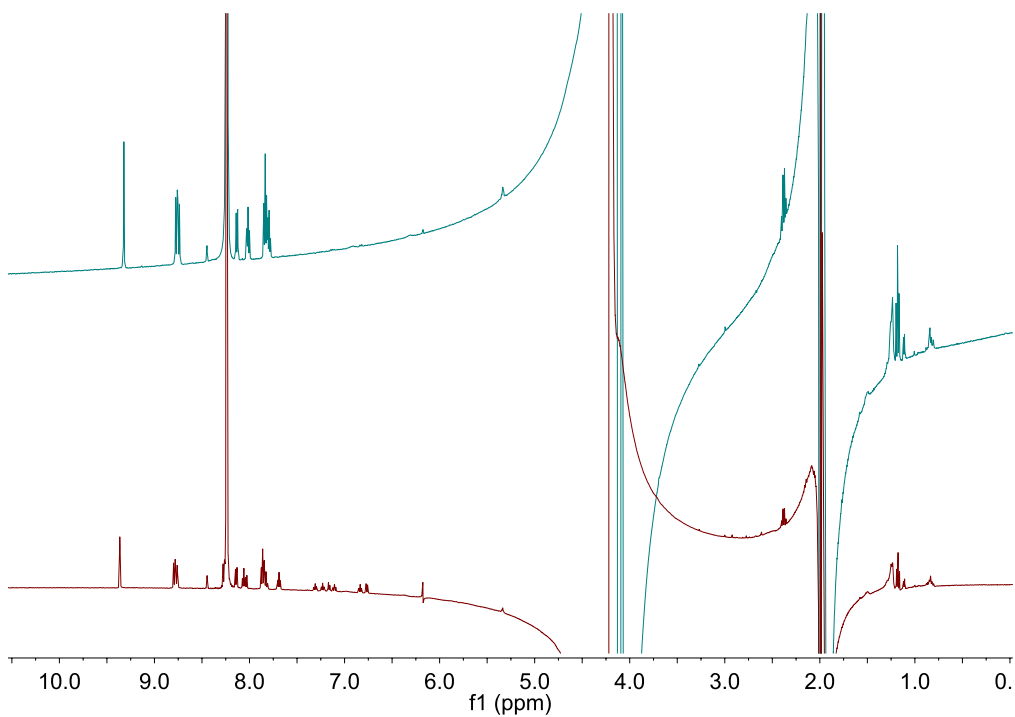


Figure S21. ^1H NMR before (blue, top) and after (red, bottom) bulk electrolysis for 1 mM **1**: 10 mM FA at Pt mesh electrode; $E_{\text{applied}} = -0.83$ V vs. $\text{FcH}^{0/+}$; 60% (v:v) $\text{H}_2\text{O}/\text{CH}_3\text{CN}$.

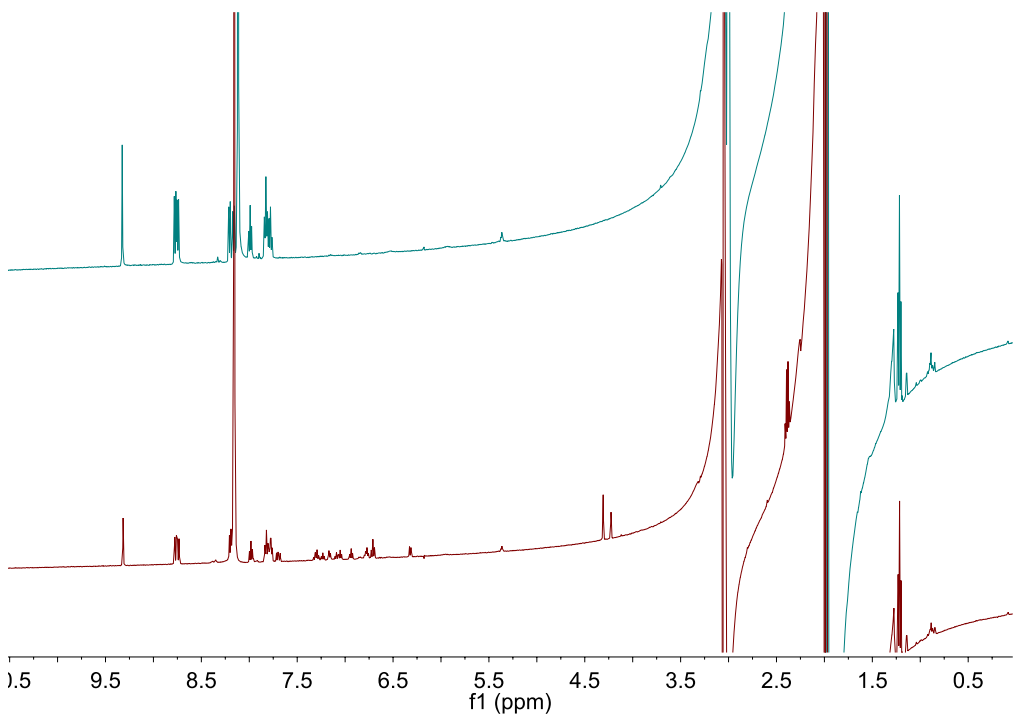


Figure S22. ^1H NMR before (blue, top) and after (red, bottom) bulk electrolysis for 1 mM **1**: 10 mM FA at RVC mesh electrode; $E_{\text{applied}} = -1.23$ V vs. $\text{FcH}^{0/+}$; 10% (v:v) $\text{H}_2\text{O}/\text{CH}_3\text{CN}$.

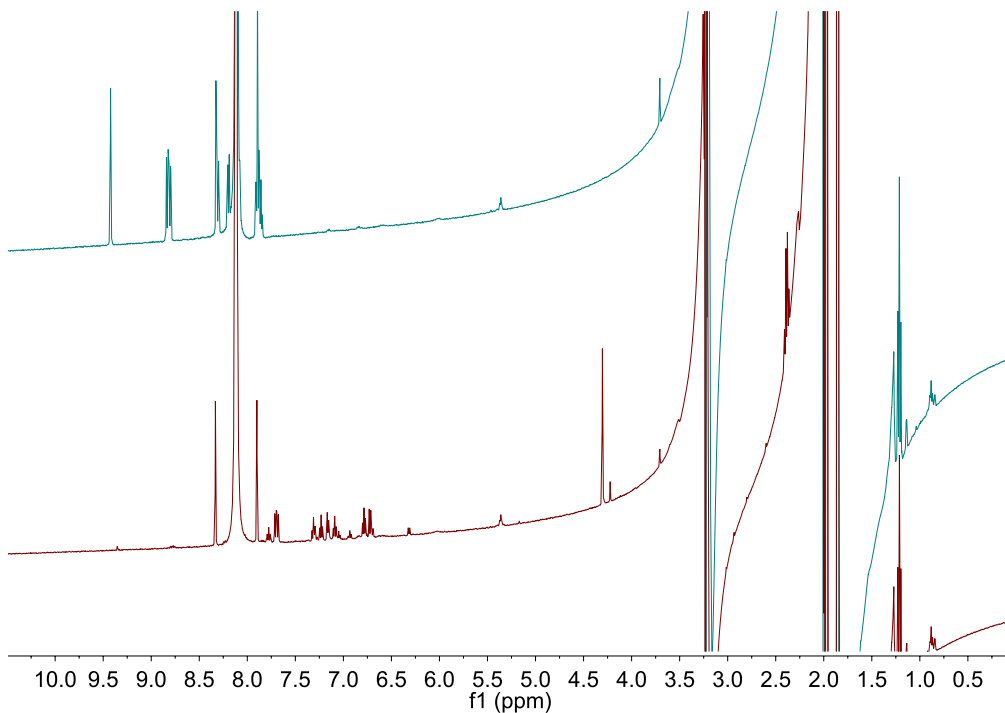


Figure S23. ¹H NMR before (blue, top) and after (red, bottom) bulk electrolysis for 1 mM **1**: 100 mM FA at RVC mesh electrode; $E_{\text{applied}} = -1.23$ V vs. $\text{FcH}^{0/+}$; 10% (v:v) $\text{H}_2\text{O}/\text{CH}_3\text{CN}$.

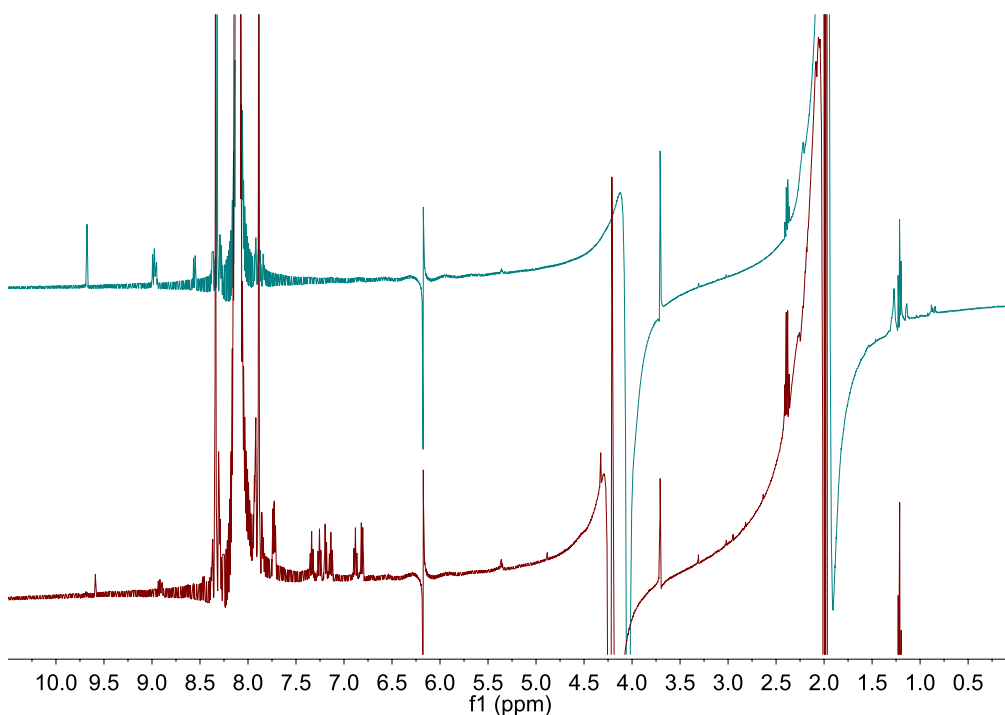


Figure S24. ¹H NMR before (blue, top) and after (red, bottom) bulk electrolysis for 1 mM **1**: 1000 mM FA at RVC mesh electrode; $E_{\text{applied}} = -1.23$ V vs. $\text{FcH}^{0/+}$; 10% (v:v) $\text{H}_2\text{O}/\text{CH}_3\text{CN}$.

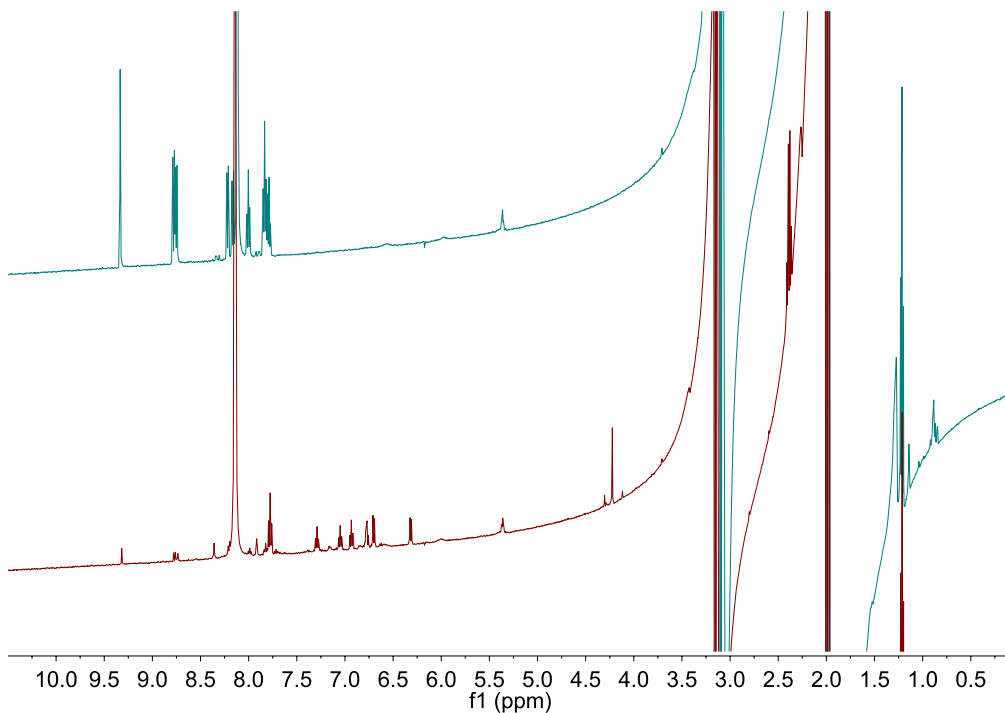


Figure S25. ^1H NMR before (blue, top) and after (red, bottom) bulk electrolysis for 1 mM **1**: 10 mM FA at RVC mesh electrode; $E_{\text{applied}} = -1.43$ V vs. $\text{FcH}^{0/+}$; 10% (v:v) $\text{H}_2\text{O}/\text{CH}_3\text{CN}$.

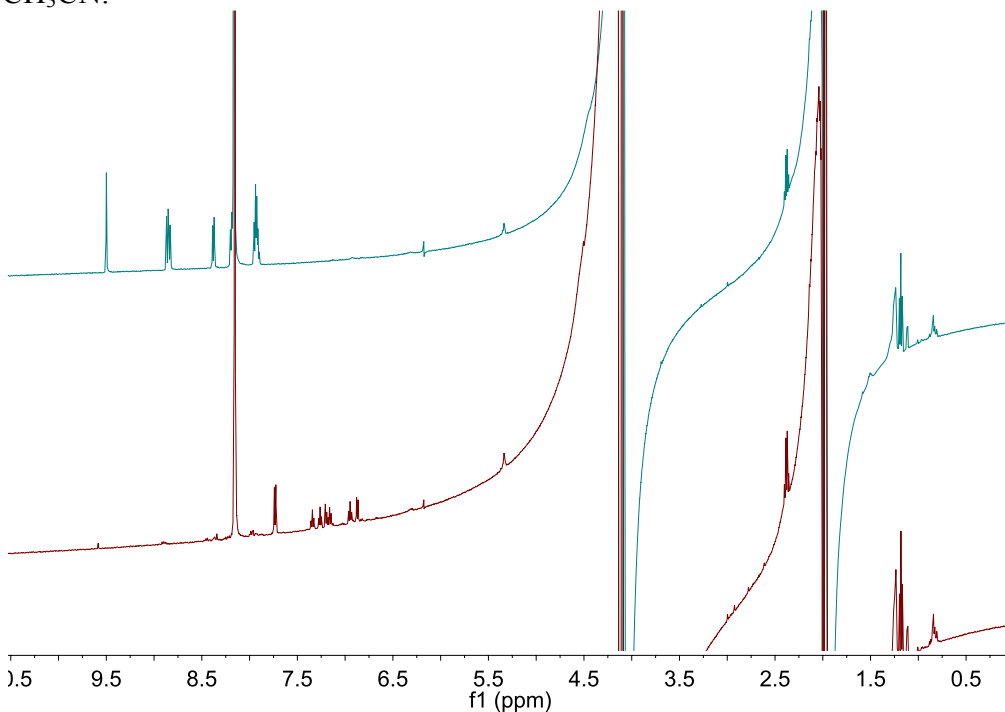


Figure S26. ^1H NMR before (blue, top) and after (red, bottom) bulk electrolysis for 1 mM **1**: 10 mM FA at RVC mesh electrode; $E_{\text{applied}} = -1.23$ V vs. $\text{FcH}^{0/+}$; 60% (v:v) $\text{H}_2\text{O}/\text{CH}_3\text{CN}$.

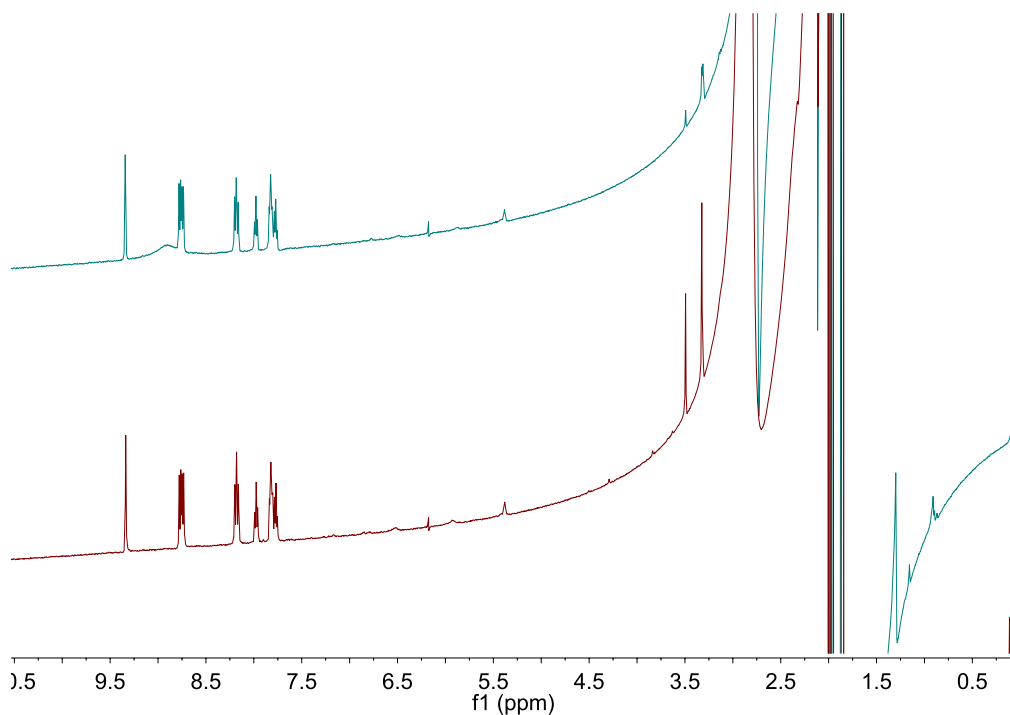


Figure S27. ¹H NMR before (blue, top) and after (red, bottom) bulk electrolysis for 1 mM **1**: 3 mM AA at RVC mesh electrode; $E_{\text{applied}} = -1.23$ V vs. $\text{FcH}^{0/+}$; CH_3CN .

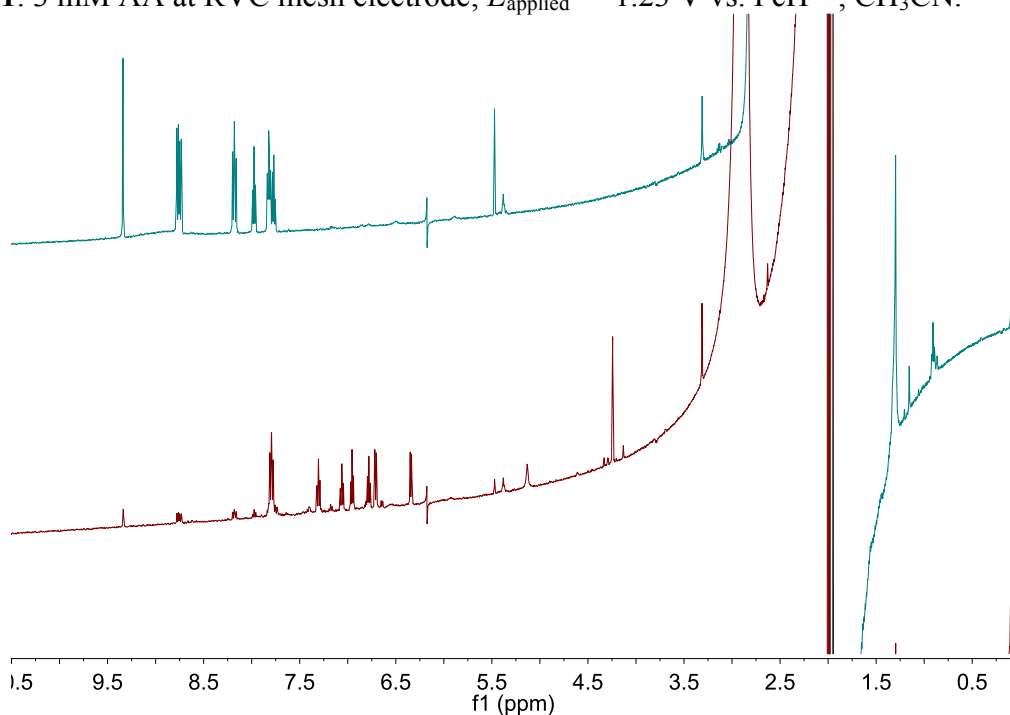


Figure S28. ¹H NMR before (blue, top) and after (red, bottom) bulk electrolysis for 1 mM **1**: 3 mM AA at RVC mesh electrode; $E_{\text{applied}} = -1.43$ V vs. $\text{FcH}^{0/+}$; CH_3CN .

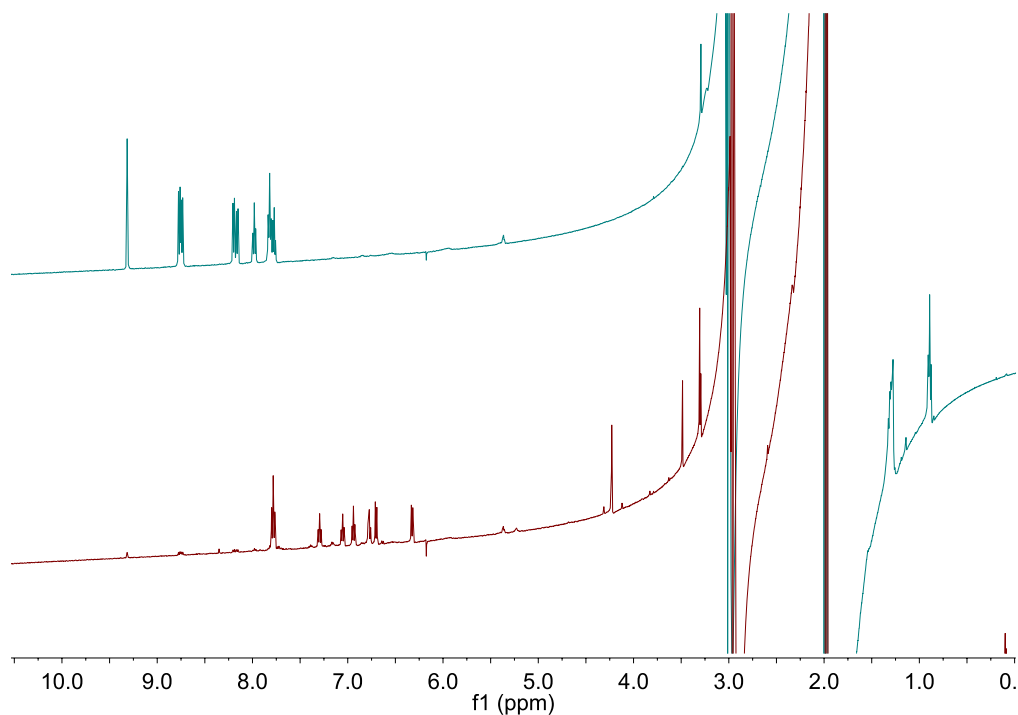


Figure S29. ^1H NMR before (blue, top) and after (red, bottom) bulk electrolysis for 1 mM **1**: 3 mM AA at RVC mesh electrode; $E_{\text{applied}} = -1.43$ V vs. $\text{FcH}^{0/+}$; 10% (v:v) $\text{H}_2\text{O}/\text{CH}_3\text{CN}$.

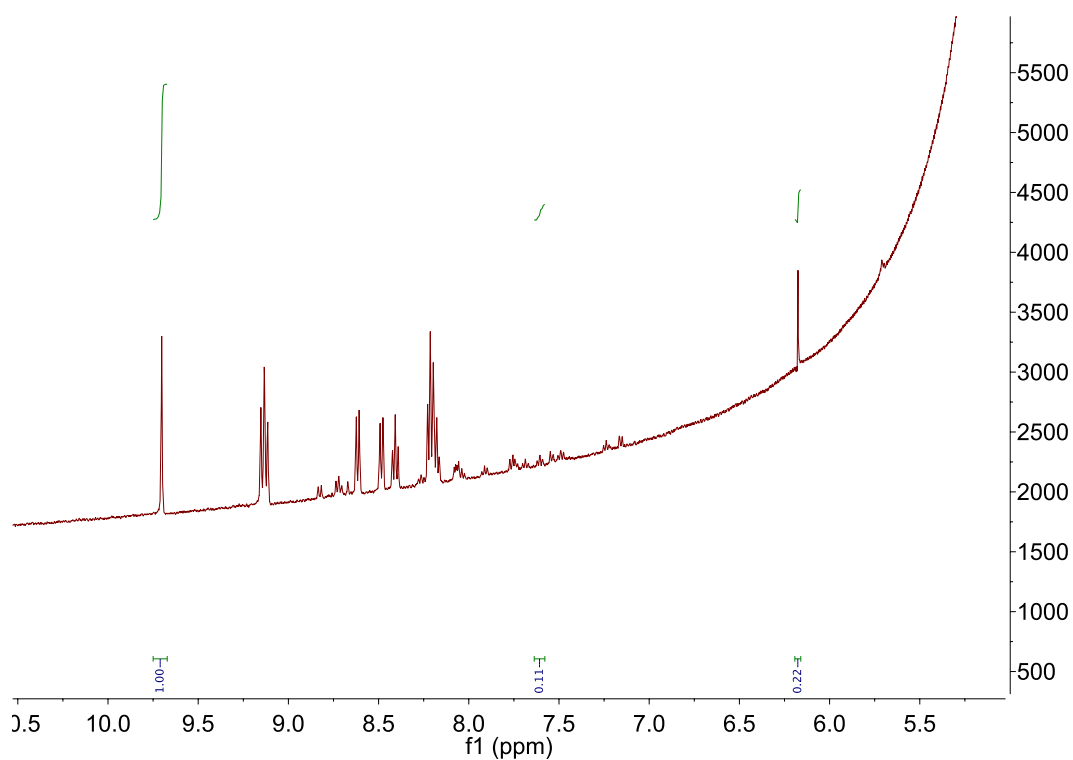


Figure S30. ^1H NMR after (red) bulk electrolysis for 1 mM **1**: 3 mM AA at RVC mesh electrode; $E_{\text{applied}} = -1.23$ V vs. $\text{FcH}^{0/+}$; 60% (v:v) $\text{H}_2\text{O}/\text{CH}_3\text{CN}$.

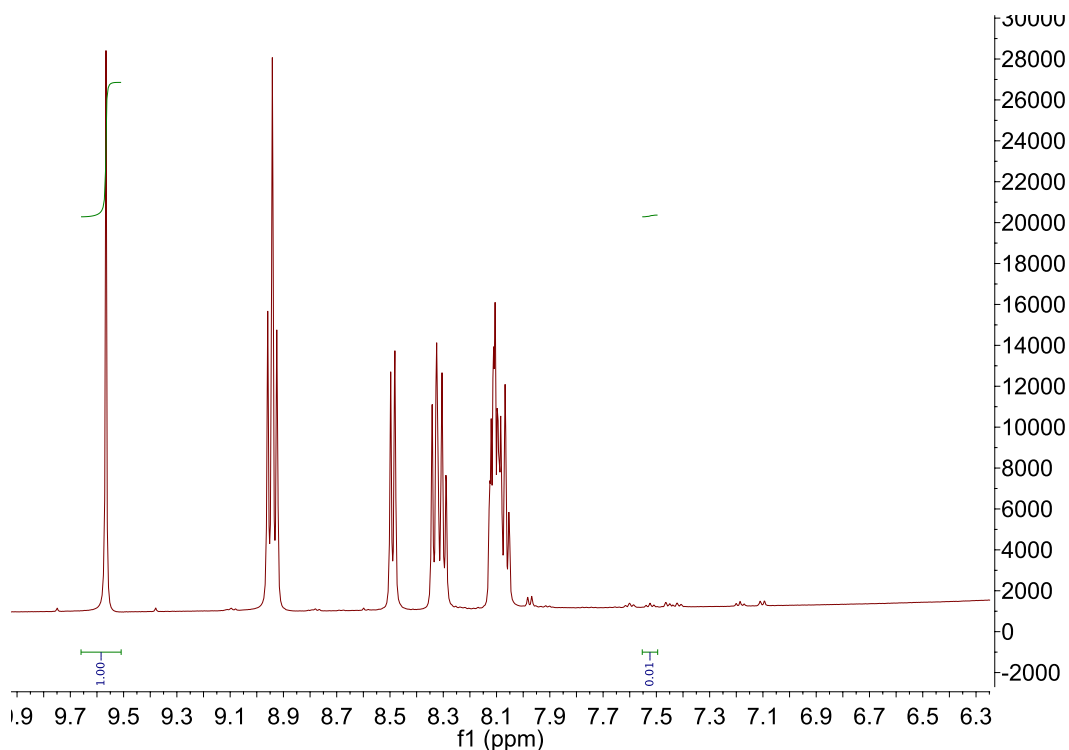


Figure S31. ^1H NMR after (red) bulk electrolysis for 10 mM **1**: 30 mM AA at Pt mesh electrode; $E_{\text{applied}} = -0.83$ V vs. $\text{FcH}^{0/+}$; 60% (v:v) $\text{H}_2\text{O}/\text{CH}_3\text{CN}$.

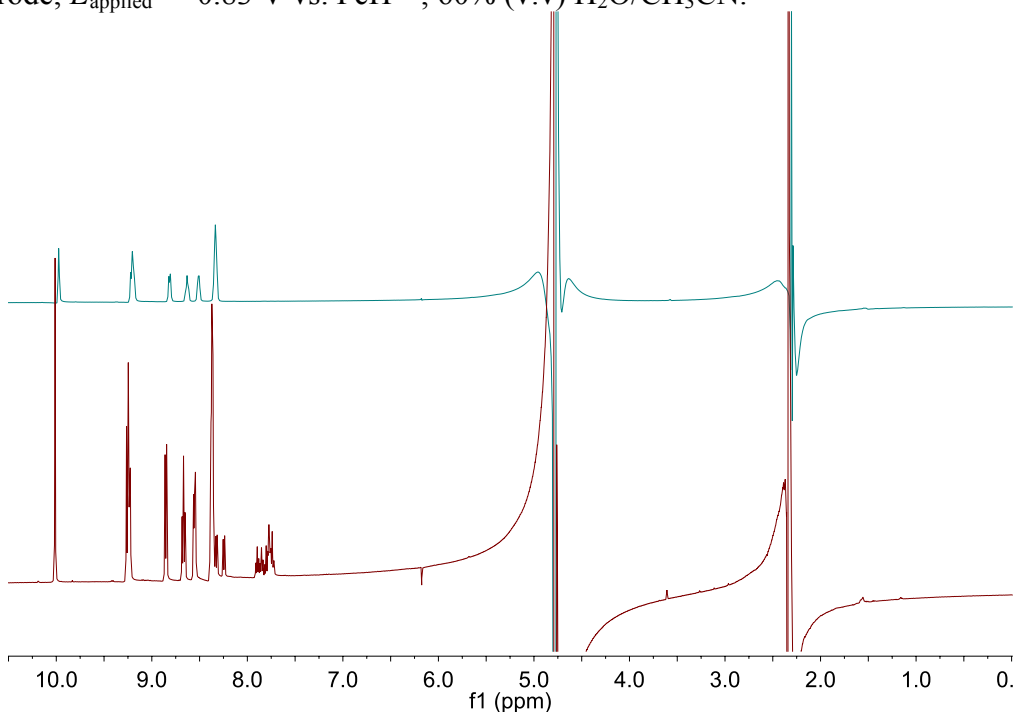


Figure S32. ^1H NMR before (blue, top) and after (red, bottom) bulk electrolysis for 10 mM **1**: 30 mM HClO_4 at Pt mesh electrode; $E_{\text{applied}} = -0.83$ V vs. $\text{FcH}^{0/+}$; 60% (v:v) $\text{H}_2\text{O}/\text{CH}_3\text{CN}$.

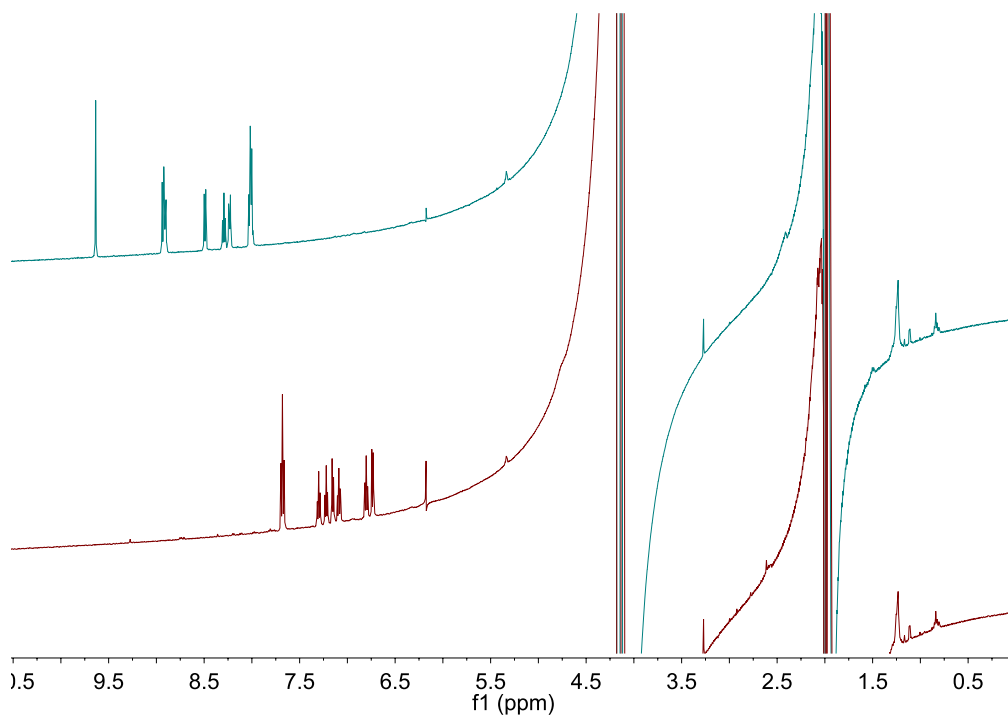


Figure S33. ^1H NMR before (blue, top) and after (red, bottom) bulk electrolysis for **1** mM **1**: 3 mM HClO_4 at RVC mesh electrode; $E_{\text{applied}} = -1.23$ V vs. $\text{FcH}^{0/+}$; 60% (v:v) $\text{H}_2\text{O}/\text{CH}_3\text{CN}$.

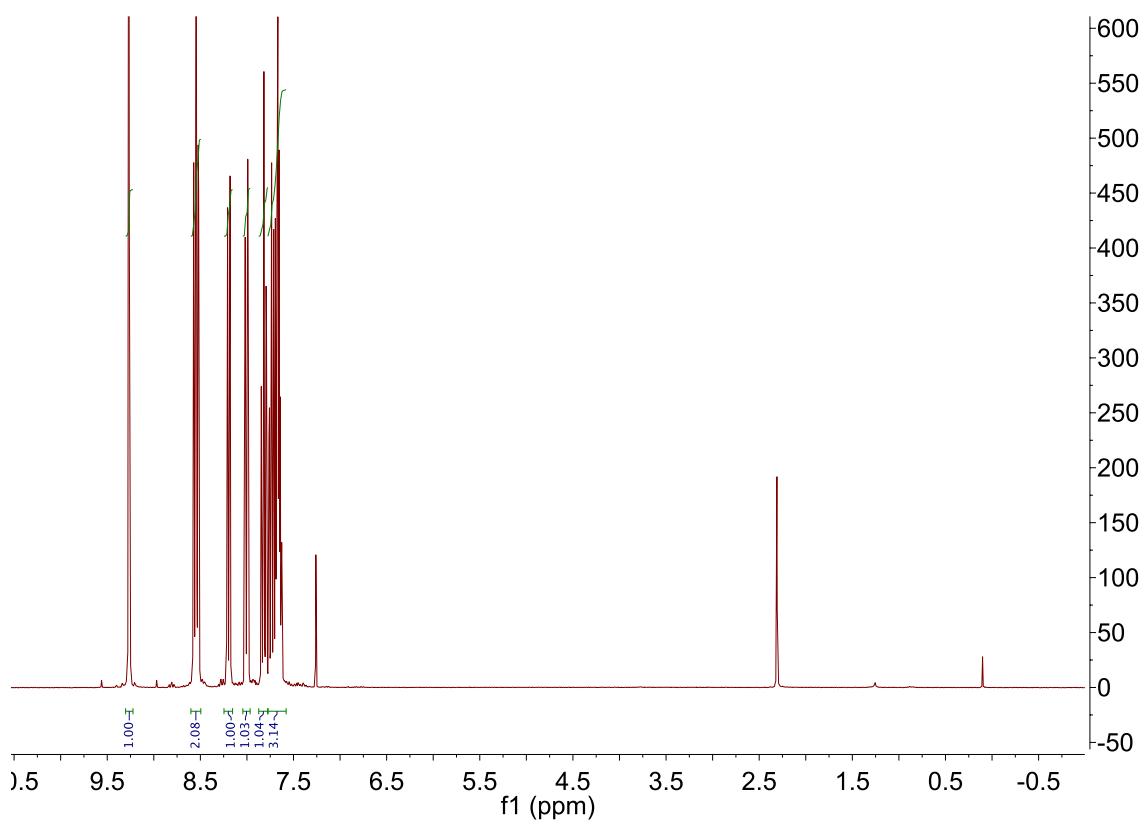


Figure S34. ^1H NMR of **1** in CDCl_3 .

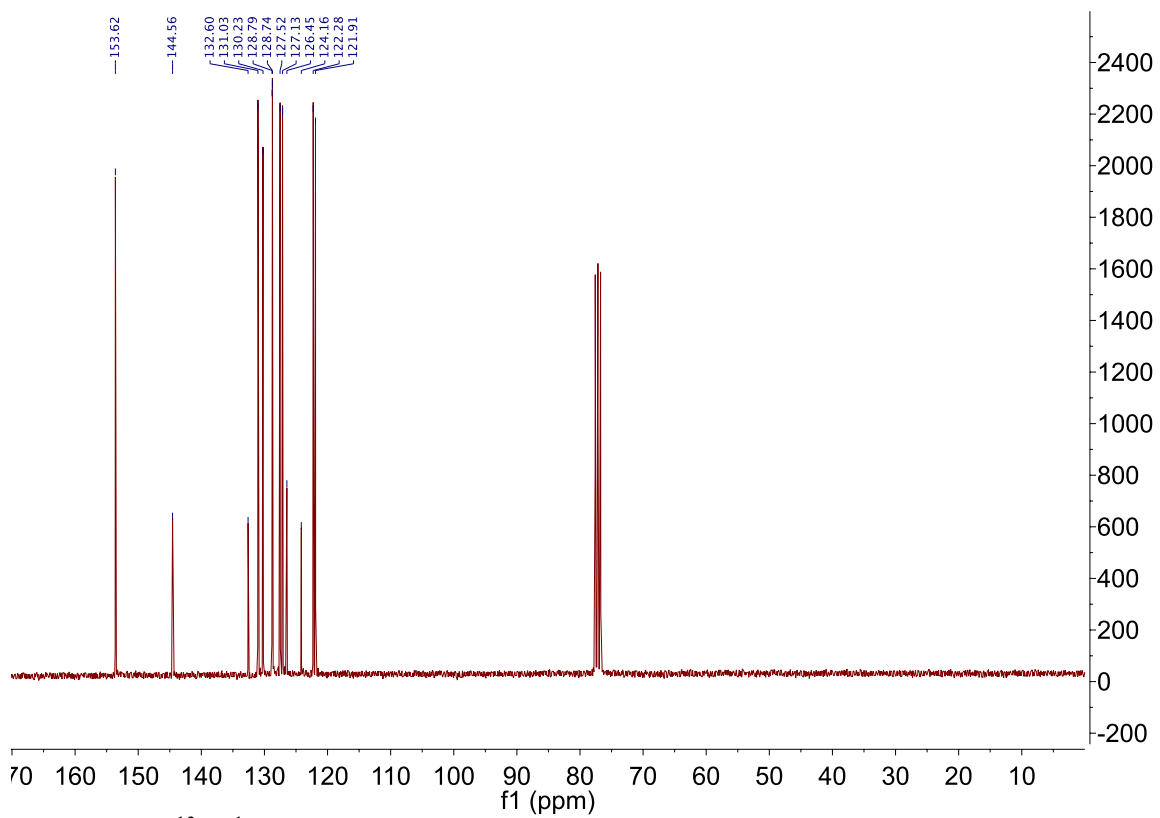


Figure S35. $^{13}\text{C}\{^1\text{H}\}$ NMR of **1** in CDCl_3 .

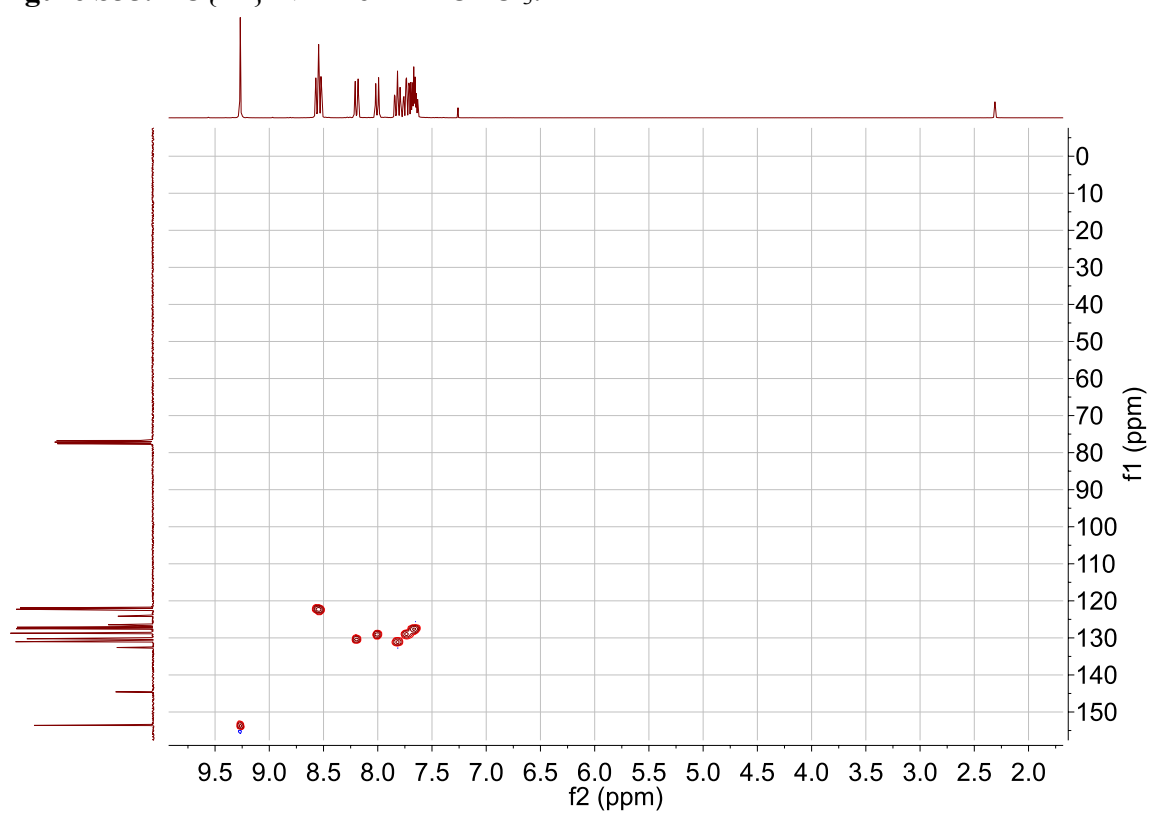
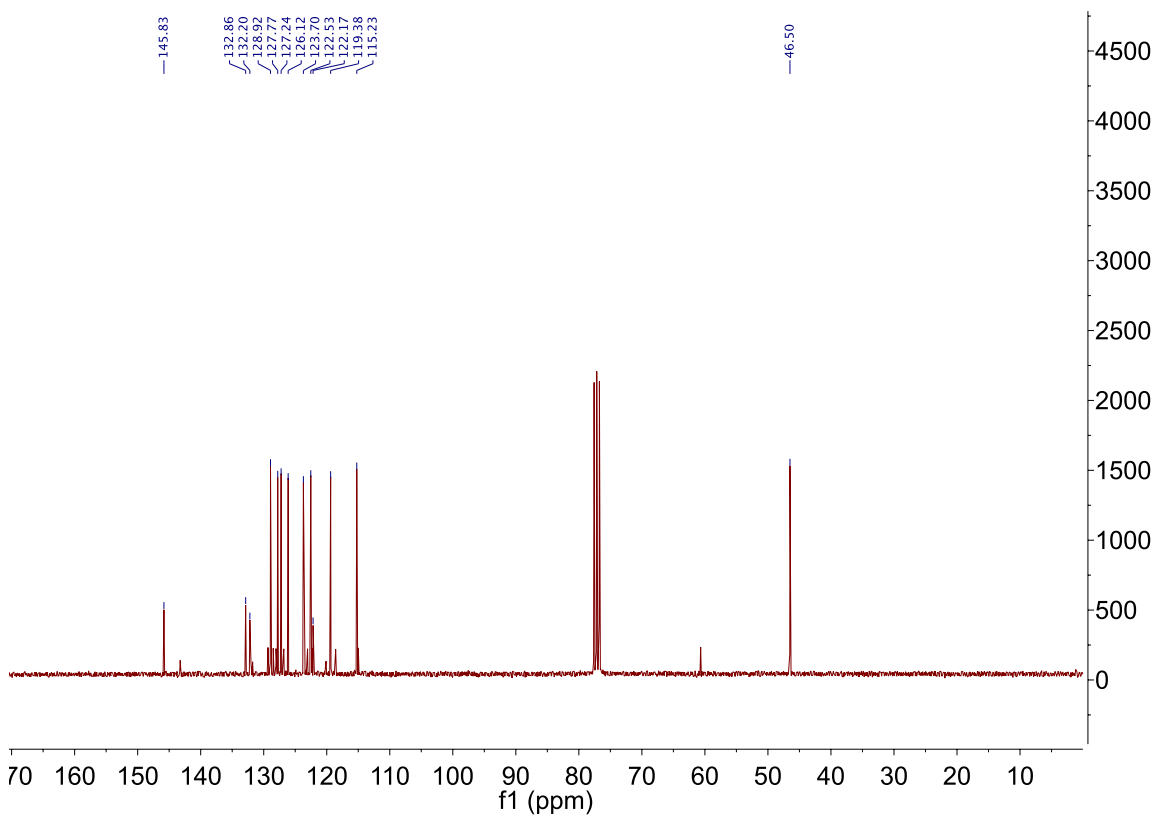
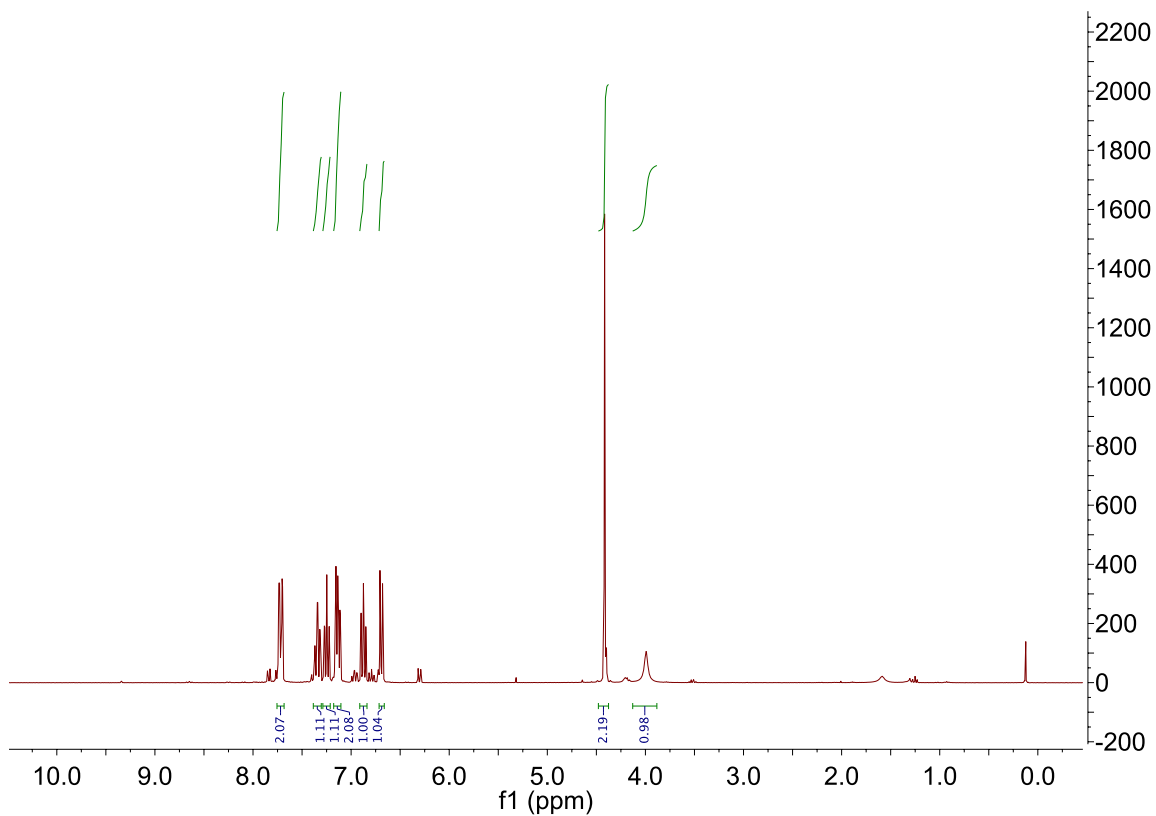


Figure S36. HSQC-DEPT of **1** in CDCl_3 .



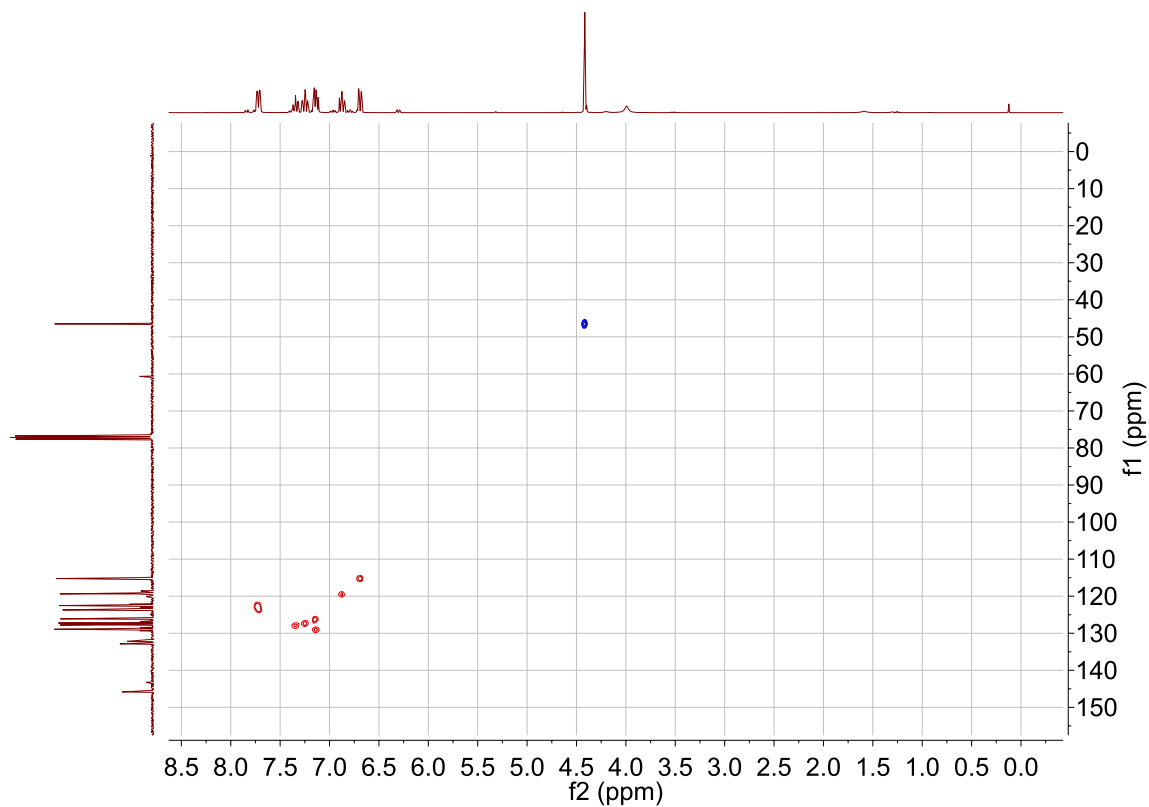


Figure S39. HSQC-DEPT of **1-H₂** in CDCl₃.

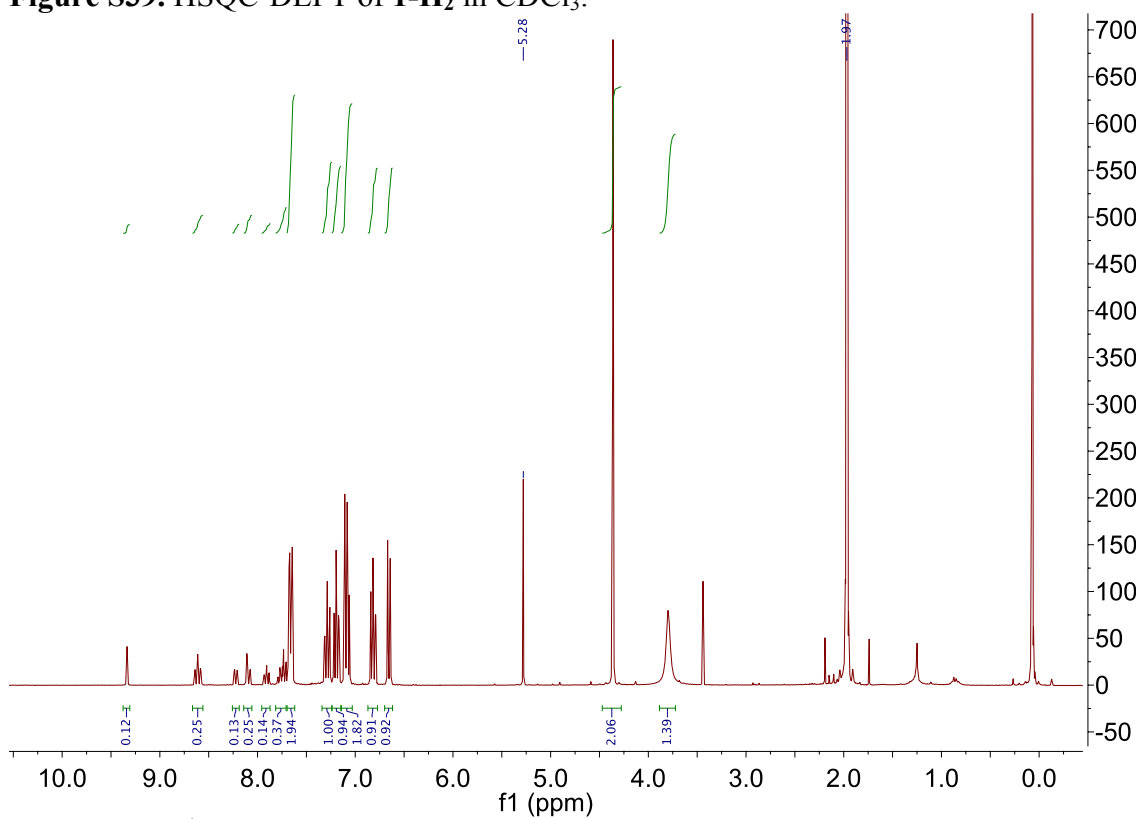


Figure S40. ¹H NMR of electrochemically generated **1-H₂**. Unreacted **1** can also be observed downfield.

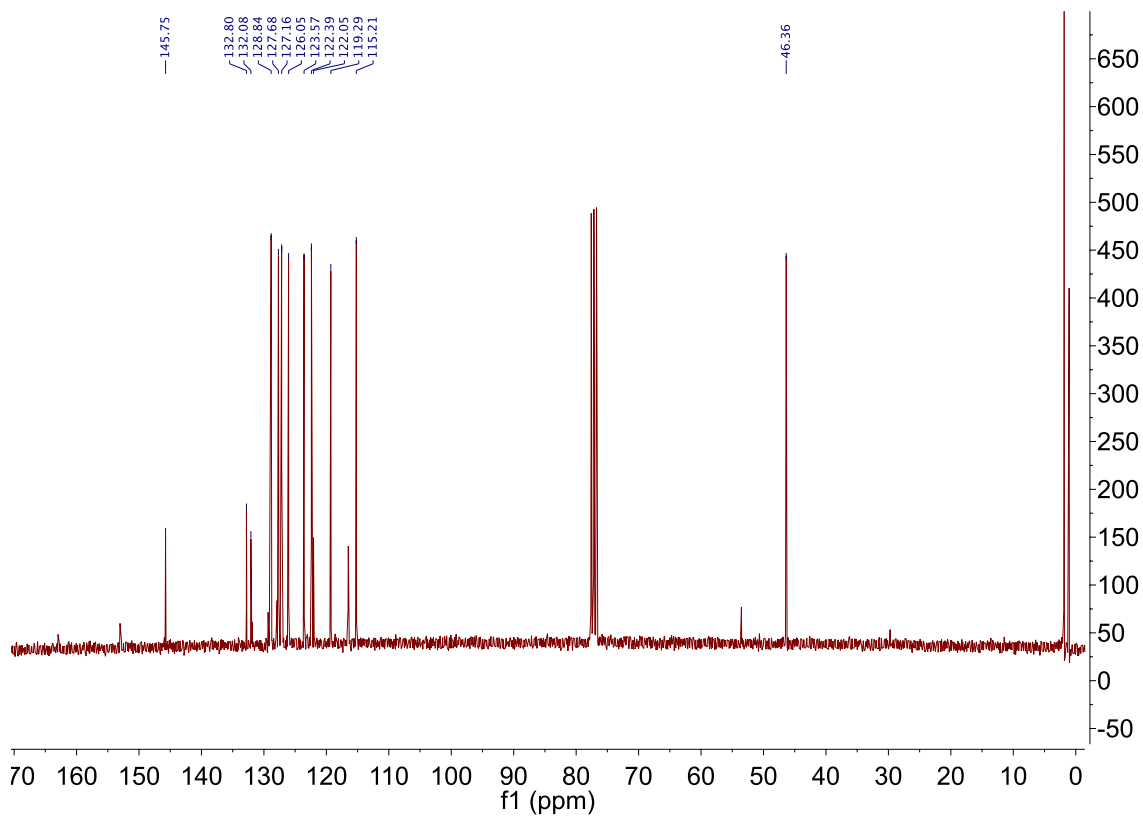


Figure S41. $^{13}\text{C}\{^1\text{H}\}$ NMR of electrochemically generated **1-H₂**.

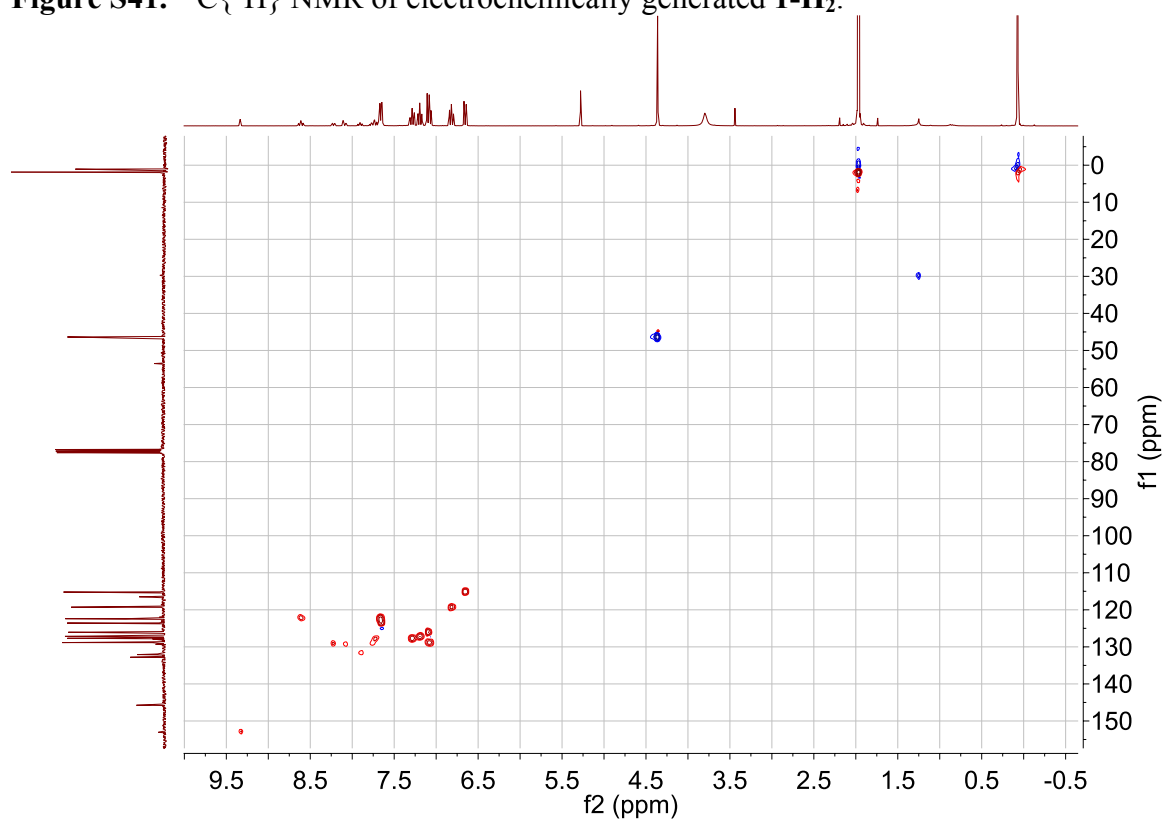


Figure S42. HSQC-DEPT of electrochemically generated **1-H₂**.

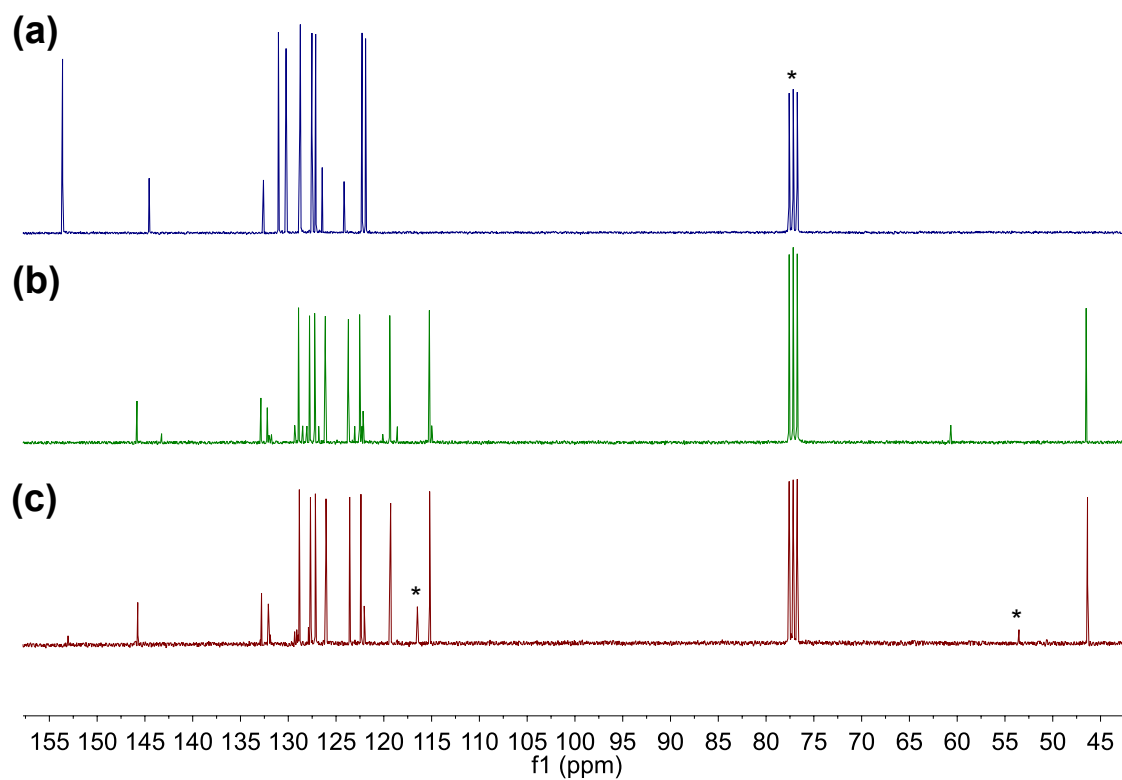


Figure S43. Stackplot of $^{13}\text{C}\{^1\text{H}\}$ NMR of (a) **1** (top, blue) synthesized, (b) chemically synthesized **1-H₂** (middle, green), and (c) electrochemically generated **1-H₂** (bottom, red) in CDCl_3 . Residual solvent peaks indicated by asterisk.

UV-VIS SPECTROSCOPY

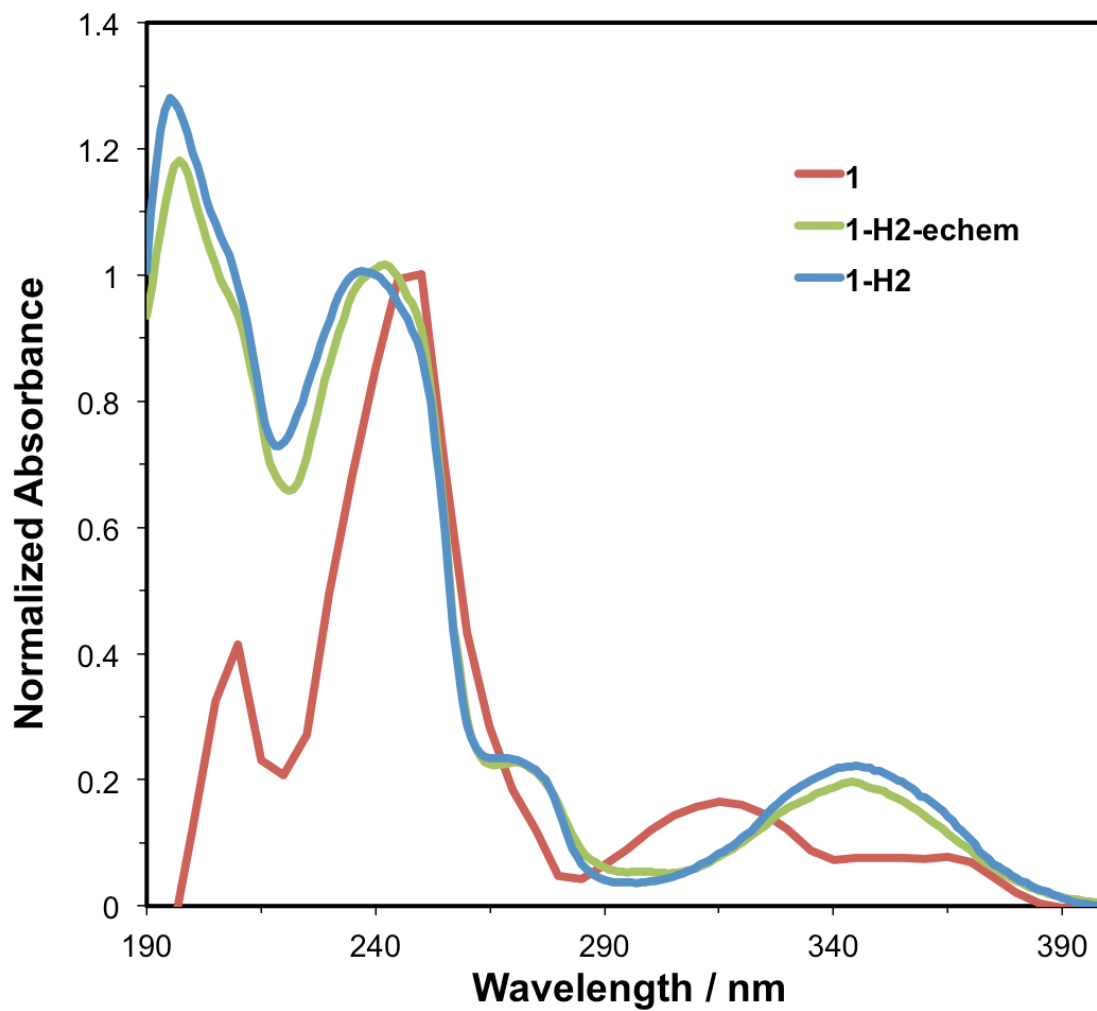


Figure S44. UV-Vis spectra of **1** (red), chemically synthesized **1-H₂** (blue), and electrochemically generated **1-H₂** (green) in CH₃CN. Absorbance spectra are normalized to the peak around 240-250 nm.

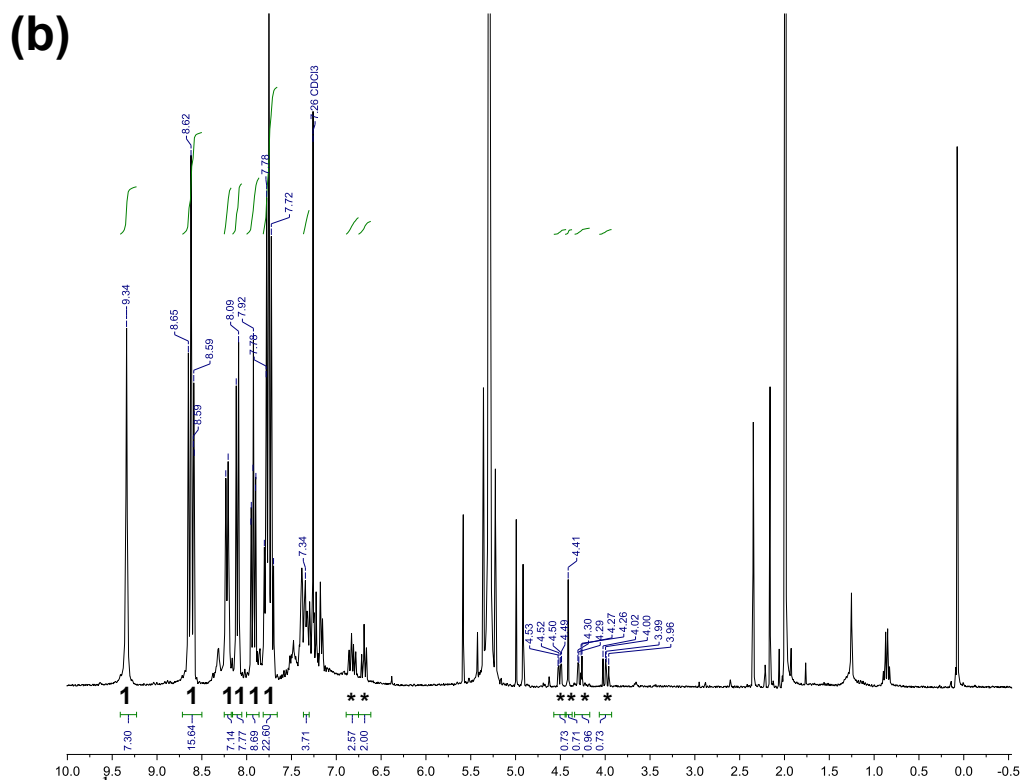
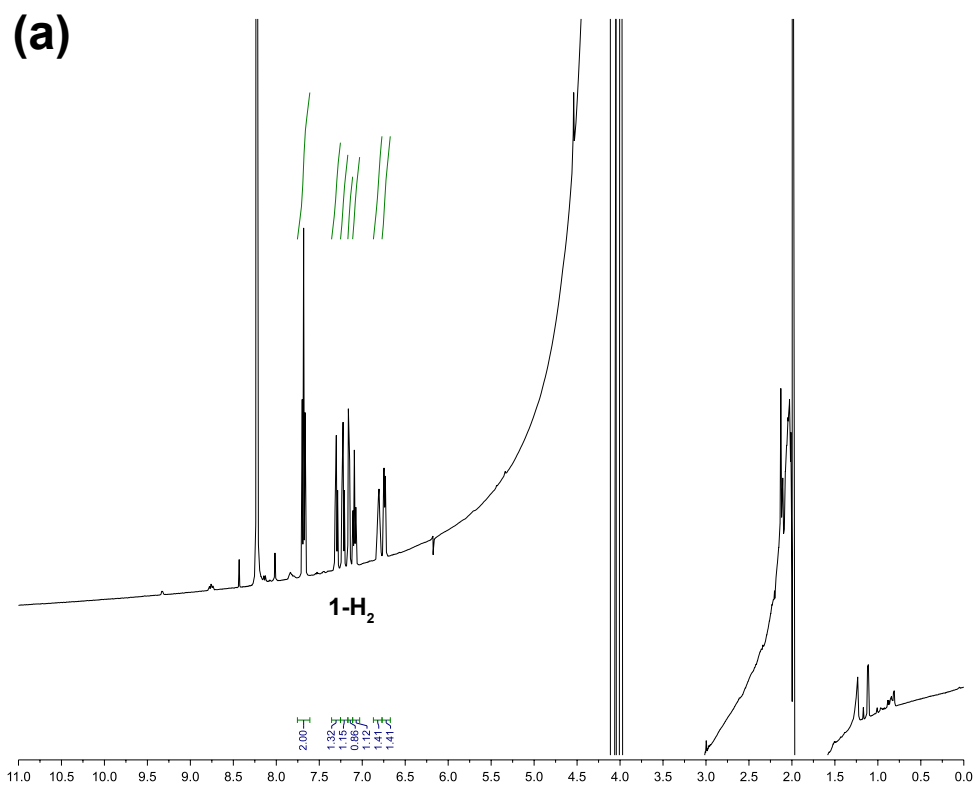


Figure S45. ¹H NMR spectra (500 MHz, 22°C) of electrochemically generated **1-H₂** (a) used in transfer hydrogenation of 3-phenyl-2*H*-1,4-benzoxazine and the crude reaction mixture (b) showing conversion to 3-phenyl-3,4-dihydro-2*H*-1,4-benzoxazine (*) and regeneration of **1**.

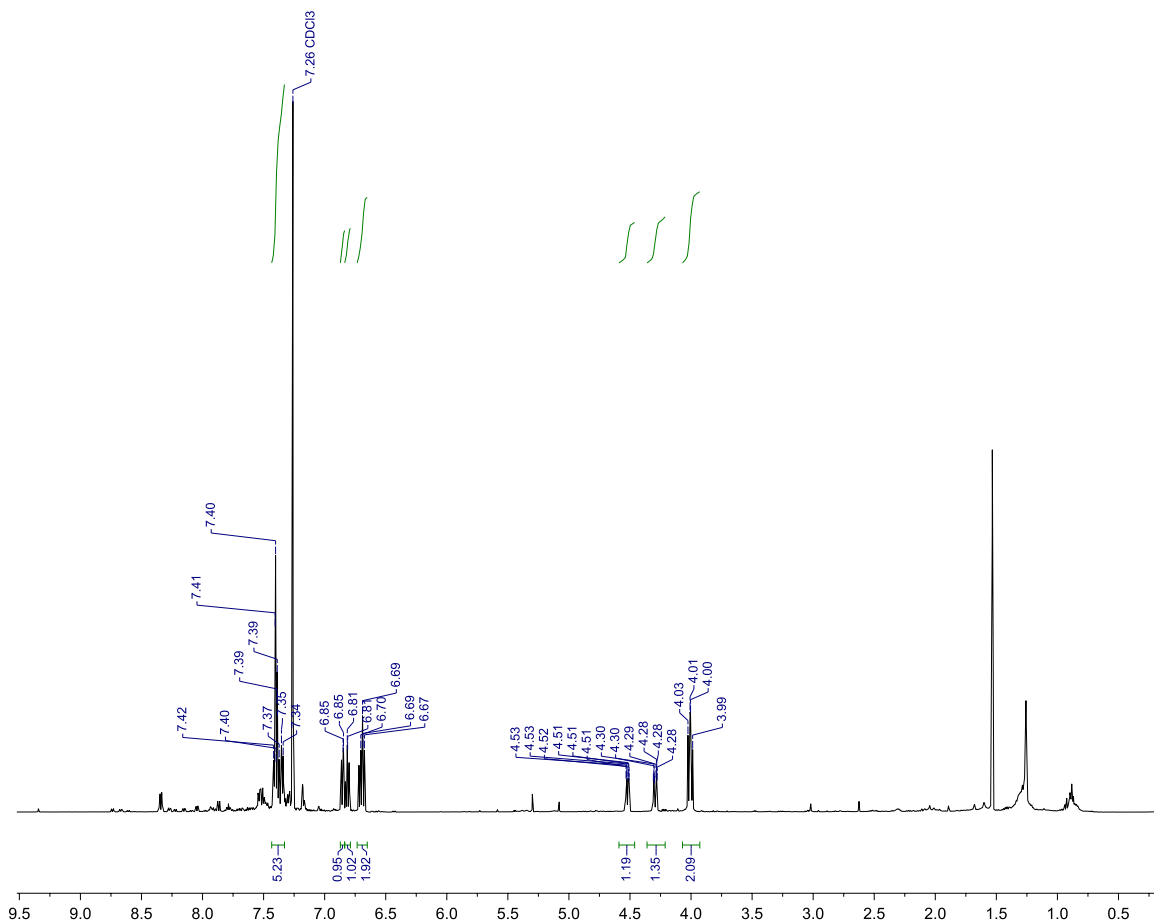


Figure S46. ^1H NMR (500 MHz, CDCl_3 , 22°C) of isolated 3-phenyl-3,4-dihydro-2H-1,4-benzoxazine generated via transfer hydrogenation using electrochemically generated 1-H_2 .